Mode Water Variability in a Model of the Subtropical Gyre: Response to Anomalous Forcing

W. HAZELEGER AND S. S. DRIJFHOUT

Royal Netherlands Meteorological Institute, De Bilt, the Netherlands

(Manuscript received 23 September 1996, in final form 5 June 1997)

ABSTRACT

The response of mode water formation to typical atmospheric forcing anomalies is studied as a possible mechanism for generating the observed interannual to decadal variability in mode water. An isopycnal model of the North Atlantic subtropical gyre, coupled to a mixed layer model, is used for this purpose. Geometry and forcing are idealized. The control run shows that mode water is a well-ventilated water mass. Formation rates up to 200 m yr^{-1} are found at the outcrop of the mode water layer. In a series of experiments the sensitivity to the position of the anomalous forcing and to the timescale of the forcing is examined. The anomalous forcing has a dipole pattern that mimics the spatial structure of the North Atlantic oscillation.

Anomalous cooling induces a positive thickness anomaly in the mode water layer at the center of the gyre and a negative anomaly at the eastern side of the gyre. The response to anomalous heat flux forcing appears to be sensitive to the position of the forcing anomaly with respect to the formation region of mode water. The formation and attenuation of the positive thickness anomaly turns out to be mainly controlled by entrainment and detrainment from the mixed layer. In the model, it takes five years to attenuate the thickness anomaly. Enhanced wind forcing generates westward propagating thickness anomalies. Adjustment takes place by long baroclinic waves. The center of the gyre, where dominant mode water variability is observed, appears to be relatively unaffected by anomalous wind forcing.

It is concluded that variability in mode water formation of the observed amplitude and timescale can be generated in the model by heat loss variations of the observed amplitude. The response to a series of heat loss events is determined by a storage mechanism by which consecutive cold winters, despite interrupting warm winters, can induce prolonged thickness anomalies in the mode water layer.

1. Introduction

In the last decade much scientific effort has been put into climate research, especially to study climate variability. The ocean is an important part of the climate system and it is thought to play an important role in low-frequency climate variability. In this article we study low-frequency variability in subtropical mode water (henceforth mode water).

Mode water is a homogeneous water mass between the seasonal and main thermocline in the subtropical gyre. It has been observed south of the Gulf Stream in the North Atlantic (Worthington 1959; McCartney 1982), where it has been given the name of 18° Water. Mode water is partly renewed at the end of each winter. Cooling over the warm Gulf Stream region in the winter and subsequent convection causes the mixed layer to deepen. When the mixed layer retreats in spring, a homogeneous water mass is left behind. This water mass has a characteristic temperature of 18°C and a salinity of 36.5 psu. The most prominent feature of mode water is its minimal vertical density gradient (thus a minimum in potential vorticity as well). After the formation, the newly formed water mass is carried away southwestward by the recirculation of the gyre, basically conserving potential vorticity.

Observations of mode water variability have been presented by Talley and Raymer (1982, henceforth TR), Dickson et al. (1996, hereafter D96), and Joyce and Robbins (1996). Using the data of Panulirus Station at Bermuda, these authors showed variability on the interannual to decadal timescales in the properties of mode water. Five periods can be distinguished in the time series of potential vorticity at Panulirus Station [see D96. Fig, 17b: the minimum of potential vorticity, here defined as $(f/\rho)(\partial\rho/\partial z)$, corresponds with the mode water core]. From 1954 to 1963 properties of mode water were nearly uniform; from 1964 to 1972 colder and denser mode water was observed. After 1972 mode water almost disappeared. In 1977 mode water was formed again with the same characteristics as in 1954. Finally, from 1985 to 1990 the mode water core shifted to a higher density. Talley and Raymer unsuccessfully tried to relate the observed mode water variability to vari-

Corresponding author address: Wilco Hazeleger, Royal Netherlands Meteorological Institute, PO Box 201, 3730 AE De Bilt, the Netherlands.
E-mail: hazelege@knmi.nl

ability in the observed surface heat flux at the formation region of mode water. The same negative result was obtained by Jenkins (1982), who focused on isopycnal salinity instead of potential vorticity. Jenkins proposed a storage mechanism by which the cumulative effect of successive winters force steady changes in mode water. Despite the results of TR, D96 attribute variability in mode water formation to variability in the atmospheric forcing. They qualitatively relate variability in convection in the west Atlantic to the North Atlantic oscillation (measured by the NAO index, the difference in sea level pressure between Iceland and the Azores). If the NAO index is low, the storm track moves southward and outbreaks of cold air occur more frequently along the U.S. East Coast. This drives enhanced formation of mode water. However, the NAO index seems to correlate much less with the potential vorticity of mode water at Panulirus after 1980 (T. Joyce 1997, personal communication).

Already in 1964, Bjerknes proposed that on the decadal timescale no simple local relationship exists between sea surface temperature (SST) anomalies and the atmospheric variability, in contrast to the shorter interannual timescale (Bjerknes 1964). The assessment of two different mechanisms of air–sea interaction operating on two different timescales was confirmed by, for example, Kushnir (1994). As mode water variability is observed to occur in between the interannual and decadal timescale, both air–sea interaction mechanisms might be operative.

If the dominant air–sea interaction on decadal timescales is most important, the ocean itself will play an active role in inducing mode water variability. In that case, mode water variability can be the result of an internal ocean mode modified by an atmospheric feedback or by an instability of the coupled system. An internal ocean mode in the subtropical gyre has been demonstrated, for example, Cox (1987) in an eddy-resolving ocean model with constant forcing. Within this model, distinct ventilation events are displayed. More recently, using concepts from dynamical systems theory, Jiang et al. (1995) and Speich et al. (1995) showed quasiperiodic behavior of the ocean in a double gyre shallow-water model. They related an instability of the wind-driven ocean circulation associated with Hopf bifurcations to interannual variability in the subtropical gyre.

Also, an instability of the coupled system may generate mode water variability. In that case a positive feedback between the atmosphere and the ocean is necessary. Such a coupled mode has been identified with a coupled GCM for the North Pacific and for the North Atlantic (Latif and Barnett 1996).

A stochastic forcing may induce variability in the thermocline (Hasselmann 1976). The spectrum of atmospheric forcing has no dominant peak in the time domain. The white noise forcing of the atmosphere can be integrated to red noise variability in the ocean. This mechanism is only possible if the typical timescale of the forcing is much smaller than the typical timescale of the responding system. If the ocean flow itself exhibits a damped oscillation as eigenmode, the damped oscillator can be excited by stochastic forcing (Griffies and Tziperman 1995).

As TR suggest, changes in the heat flux and water characteristics far from the northern Sargasso Sea may also affect the formation of mode water. Such a nonlocal mechanism will not be studied here.

The dominant air–sea interaction on interannual timescales is forced by atmospheric variability that generates surface heat flux anomalies (Cayan 1992). The heat flux anomalies determine changes in mixed layer depth and thermocline ventilation, associated with anomalous mode water formation. This local air–sea interaction mechanism will be investigated in this study. In order to get a better understanding of the variability displayed in the Panulirus time series we will determine the typical amplitude and timescale of anomalies in mode water generated by the different mechanisms mentioned above. In the present study we will focus only on the response of mode water formation to anomalous atmospheric forcing in a series of experiments.

To investigate the role of local air–sea interaction mechanisms in generating mode water variability a numerical ocean model is used with mixed layer physics included. In later studies this model will be adapted in order to assess the relative role of the several mechanisms mentioned above. The numerical model is an isopycnic general circulation model. Some advantages of using an isopycnic ocean model for this type of experiments have been stated before by Drijfhout (1994a); that is, mixing in the ocean as well as in the model occurs mainly along isopycnals and potential vorticity is largely conserved on isopycnals. Moreover, water masses are unambiguously defined within the model context, for example, 18° Water corresponds with the 18°C layer in the model. Finally, subduction, which is the process by which fluid transfers from the mixed layer into the thermocline, can be explicitly calculated (see section 3b). Woods (1985) showed that shoaling of the mixed layer is essential for a correct simulation of thermocline ventilation. Also the seasonal cycle in mixed layer depth needs to be resolved to capture late winter ventilation (Williams et al. 1995). Therefore, the isopycnic model is coupled to a Kraus–Turner mixed layer model (Bleck et al. 1989) and the seasonal cycle in the forcing is resolved. Because we want to emphasize processes, a simple model configuration is used (see section 2a).

The dominant mode of variability in the atmosphere in the North Atlantic region is characterized by a dipole in the pressure distribution, the well-known North Atlantic oscillation (NAO). Therefore, the model is forced with idealized anomalous forcings that mimic the NAO. We have applied anomalous wind stress as well as anomalous heat flux forcings separately and together (see

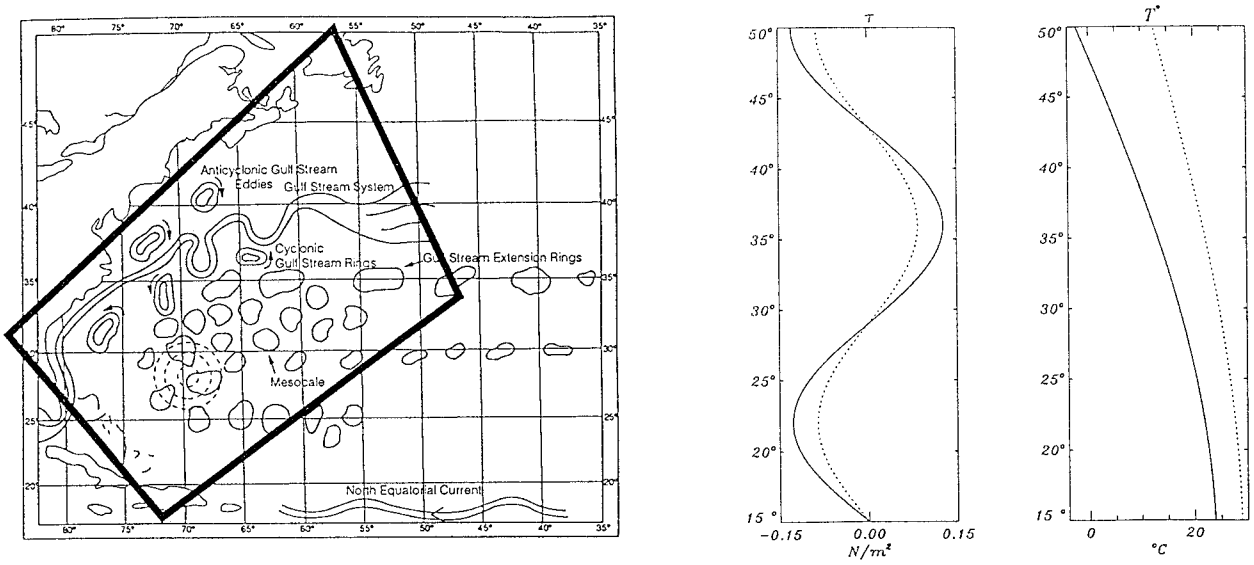

FIG. 1. The domain of the model, the zonal wind stress, and the zonal apparent temperature (stippled: summer, solid: winter).

section 2b). Both forcing fields are based on observational patterns of variability. The anomalous forcings are applied for 1 and 10 yr; the latter is a typical timescale for mode water variability. In some experiments severe outbreaks with a 5-day period are simulated. Anomalous heat flux forcing experiments have also been conducted by Marsh and New (1996). They used climatological data to force a realistic ocean model of the North Atlantic and performed some experiments with additional anomalous forcings. It was found that five years of anomalous forcing induced a strong negative potential vorticity anomaly in their mode water layer. In contrast to TR they showed that a typical anomalous heat flux forcing induces mode water variability of the observed amplitude. They hypothesize that this discrepancy with the results of TR was probably due to the fact that TR used a too small area for calculating the anomalous heat flux. However, a storage mechanism might also explain the weak correlation between mode water variability and the heat flux variability.

The present study uses idealized geometry and forcing. This enables us to emphasize more on processes, to distinguish between separate timescales of the anomalous forcing, to study the sensitivity to the position of the anomalous forcing, and to distinguish between anomalous wind forcing and heat flux forcing. We are also able to separate the response during the anomalous forcing and afterward. Moreover, the anomalous forcing experiments will serve as a standard to compare the relative role of other mechanisms for generating mode water variability.

A short description of the numerical model and the control forcing is given in the next section, followed by a description of the anomalous forcings. In section 3 the results of the control run are shown with specific attention to water mass formation. Section 4 describes the results of the experiments with anomalous forcings followed by a discussion in section 5. We summarize and draw conclusions in section 6.

2. Experimental setup

a. The numerical model and the control forcing

In this study an extended version of the model described by Drijfhout (1994a,b) is used. It is a three-dimensional isopycnic primitive equation model based on the model of Bleck and Boudra (1986). The same domain is chosen as in Drijfhout (1994a,b) as this captures the main features of the North Atlantic subtropical gyre (Fig. 1). The lateral boundaries are closed. This is reasonable because we study interannual to decadal variability, which is closely related to the gyre circulation. Moreover, we focus in this study on the role of local air–sea interaction mechanisms. Bottom topography includes a continental shelf break (Drijfhout 1994a; Semtner and Mintz 1977). There are seven isopycnic layers in the model, with a temperature difference of 4°C between each layer, starting with 2°C in the deepest layer. The horizontal resolution is 74 km. Salinity is kept constant, and a linear equation of state is used in these experiments. Eddies are not resolved with this resolution and a Laplacian friction is used to parameterize subgrid phenomena. The viscosity parameter is 3×10^3 m^2 s^{-1} and the diffusive parameters for temperature and layer thickness are 1.5×10^3 m^2 s^{-1}. Furthermore, a small cross-isopycnal diffusion with a diffusivity of 1 cm^2 s^{-1} is incorporated, according to Huang and Bryan (1987). Convection is parameterized with convective adjustment.

The main difference between the model described by Drijfhout (1994a,b) and the model used here is the in-

clusion of a mixed layer on top of the seven isopycnic layers. When coupling a mixed layer model to an isopycnic model, it is most appropriate to use a bulk mixed layer model. With this choice the vertical structure of homogeneous layers in the isopycnic model is retained. We use a Kraus–Turner mixed layer model based on the algorithm described by Bleck et al. (1989). Bulk mixed layer models have been used successfully in many ocean models (e.g., Sterl and Kattenberg 1994; Marsh and New 1996). Compared to more sophisticated mixed layers models, bulk mixed layer models simulate the observed mixed layer depth and SST very well (see Martin 1985 for a comparison with a second-order closure model). Some minor adjustments in the detrainment algorithm have been made to avoid very thin mixed layers. First, the incoming heat is distributed over the upper 20 m if the mixed layer thickness becomes smaller than 20 m. In that case, part of the heat is used for a mass exchange between the two uppermost isopycnic layers beneath the mixed layer. Second, the turbulent kinetic energy input by the wind has been made a function of the ratio of the mixed layer depth to the Ekman depth (here defined as $0.4\,u_*/f$, see Sterl and Kattenberg 1994). Finally, the Ekman depth is used as the depth to which the mixed layer detrains when the Monin–Obukhov length becomes smaller than the Ekman depth.

An age tracer is included in the model. This is a passive tracer that is set to zero when it enters the mixed layer and gets older with time beneath the mixed layer. In order to find age, the same advection diffusion equation as used for the temperature is integrated. Diapycnal diffusion, convective adjustment, and detrainment/entrainment from and into the mixed layer are taken into account.

The model is driven by a zonally averaged wind stress and by a buoyancy flux. The latter is obtained by relaxing the SST to a zonally averaged apparent temperature. The restoring time constant is equal to 20 days times the mixed layer depth divided by 50 m. The wind stress profile has an idealized sinusoidal form, which results in a 2½ gyre circulation in the basin. Both the wind stress and buoyancy forcing resolve the seasonal cycle (see Fig. 1). The amplitude of the forcing varies sinusoidally between the extremes in the winter and the summer.

As the basin width at the latitude of the maximum anticyclonic wind stress curl is about one-third of the width of the subtropical Atlantic, the amplitude of the wind stress has been enhanced by a factor of 3. In this way, the linear component of the western boundary current will have the correct magnitude. The horizontal mass transport is now $O(50\ \text{Sv})$ ($\text{Sv} \equiv 10^6\ \text{m}^3\ \text{s}^{-1}$). The advective timescale of the subtropical gyre, however, is much too short due to the small basin, that is, one to two years. To correct for this deficiency and to obtain a realistic ratio between advection and forcing timescales, the seasonal cycle is shortened by a factor of 3. The overall flow field and thickness distribution appeared to be rather insensitive to this change. The formation rates and renewal times became far more realistic; that is, the formation rate of mode water became 6 Sv, compared to about 20 Sv with the long seasonal cycle (note that due to the small basin of the model, the formation rate must be less than observed) and the renewal time became 6 years, compared to 2 years respectively. When referring to years in this study, we mean one seasonal cycle.

b. Anomalous atmospheric forcings

A series of experiments with anomalous atmospheric forcings is performed with a duration of 1 and 10 yr. The surface heat flux applied to the ocean model in the anomalous cooling experiments is

$$H = H_{\text{obs}} + \gamma(T_{\text{obs}} - T) + H_{\text{anom}}.$$

Here H_{obs} and T_{obs} are the diagnosed heat flux and SST obtained after an extensive spinup with restoring boundary conditions, T is the SST, γ is a relaxation coefficient (see section 2a), and H_{anom} is the anomalous heat flux.

The spatial patterns and the amplitudes of the anomalous heat flux are based on the dominant modes of variability in the heat flux as presented by, for example, Cayan (1992, Fig. 7). A dipole structure, typical for interannual variability in the North Atlantic, emerges in his EOFs. These anomalies are strongest in the winter. The same patterns have been obtained by Kushnir (1994). He showed that warm SSTs in midlatitudes and high latitudes are associated with cold temperature anomalies in the subtropics. He also showed an inverse correlation between interannual fluctuations of midlatitude SST and the strength of the overlying westerlies. The variability in the westerlies is related to the dominant mode of variability in the atmosphere in the North Atlantic region. This dominant mode, also known as the North Atlantic oscillation, is characterized by a dipole pattern in the pressure distribution: the anomalously strong Iceland low pressure area coincides with the anomalously strong Bermuda high and vice versa. The spatial pattern of the NAO is approximated by two-dimensional Gaussian patterns for the anomalous wind and heat flux forcing.

In the anomalous heat flux forcing experiments, only the southern part of the dipole has been used, as the northern pole did not have any effect on the mode water formation. The patterns shown in Figs. 2a–c, depict the variability in the heat flux forcing. The maximum anomalous heat loss is 200 W m^{-2}. The patterns shown in Figs. 2a and 2b (corresponding to experiment I and II, see Table 1) are applied for one winter, in order to study the sensitivity to the position of the heat flux anomaly and to study the formation and attenuation of the generated thickness anomalies in mode water. To study longer term variability the pattern shown in Fig. 2c is applied for ten consecutive winters. In the summer the amplitude of the anomalous forcing vanishes, and in the

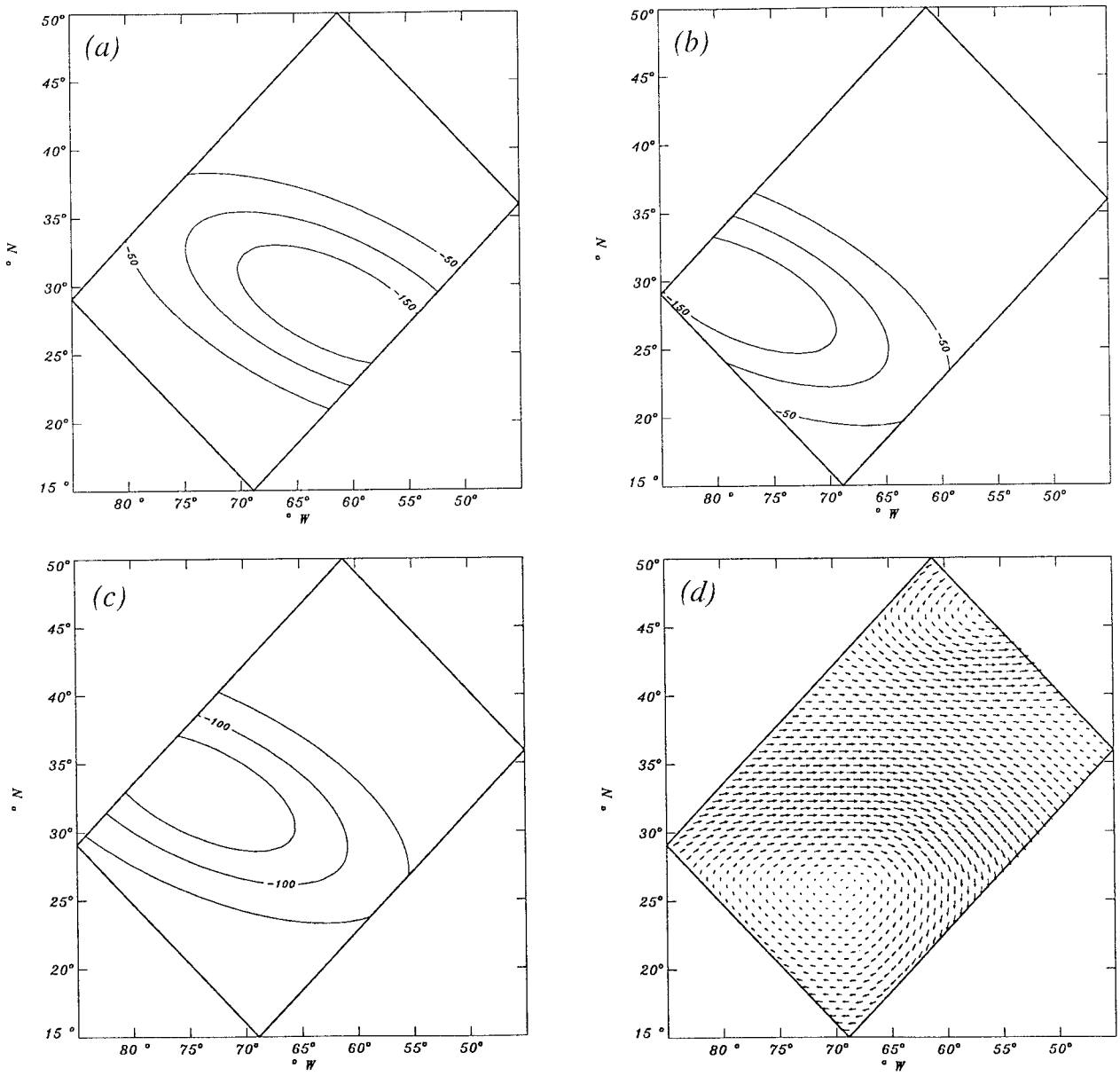

FIG. 2. Patterns of anomalous heat flux (W m^{-2}) in (a) the eastern Atlantic (expt. I), (b) the southwestern Atlantic (expt. II), and (c) the western Atlantic (expts. III, IV, V, VII, and X). (d) Pattern of anomalous wind forcing (maximum 2 m s^{-1}; expts. VIII, IX, and X).

TABLE 1. Experiments.

	Pattern	Maximum amplitude	Duration
I	Fig. 2a	−200 W m^{-2}	1 yr
II	Fig. 2b	−200 W m^{-2}	1 yr
III	Fig. 2c	−200 W m^{-2} (regime shift)	10 yr
IV	Fig. 2c	−200 W m^{-2} (gradual)	20 yr
V	Fig. 2c	0 W m^{-2} (outbreaks*)	10 yr
VI	Fig. 2c	−200 W m^{-2} (outbreaks*)	10 yr
VII	Fig. 2c	Derived from historical data	25 yr
VIII	Fig. 2d	2 m s^{-1}	1 yr
IX	Fig. 2d	2 m s^{-1}	10 yr
X	Fig. 2c + 2d	−200 W m^{-2}, 2 m s^{-1}	10 yr

* Outbreaks have a 5-day period with a maximum of −800 W m^{-2}.

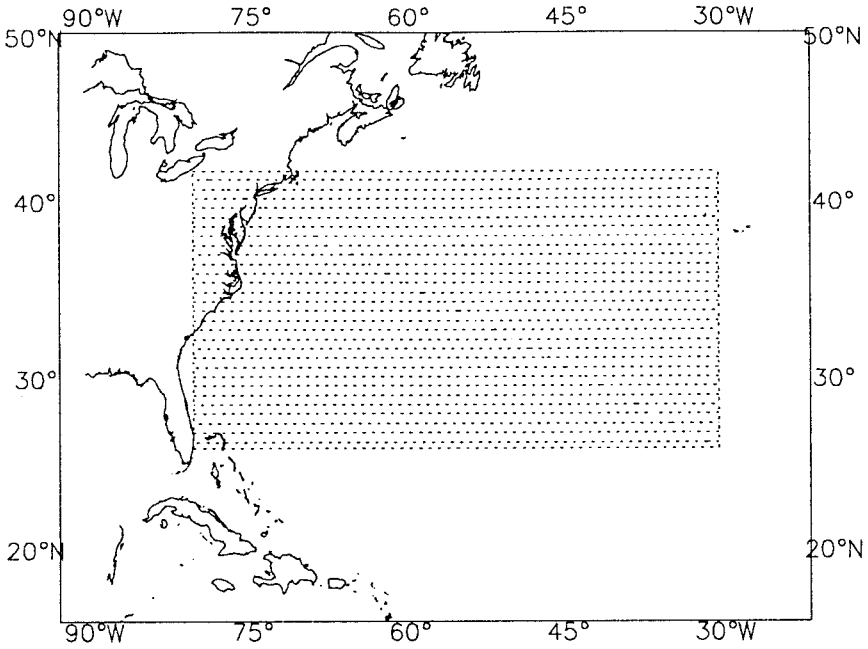

FIG. 3. Area used to determine observed anomalous heat fluxes.

winter the amplitude gradually increases to a maximum of -200 W m^{-2} (experiment III). A ''gradual NAO'' experiment has been performed by applying the anomalous forcing for 20 years. Again, each winter the pattern is switched on. In this experiment the maximum amplitude of the forcing varies sinusoidally with a period of 20 years (i.e., 10 cold years followed by 10 warm years, experiment IV). This enables us to distinguish between gradually changing forcing and sudden regime shifts. Talley and Raymer reported that variability in the heat loss in the Sargasso Sea is due to frequent outbreaks of cold and dry air from the American continent. To simulate such outbreaks two experiments with an anomalous forcing are conducted with the same period and pattern as in experiment III, but the amplitude is changed. In experiment V, during the first 5 days of the month the maximum amplitude was -800 W m^{-2}; during the rest of the month the maximum amplitude was 160 W m^{-2}. This results in a vanishing monthly averaged anomalous forcing. In another experiment the same strategy is followed, but a maximum amplitude of -80 W m^{-2} is used instead of 160 W m^{-2} during ''normal'' conditions (experiment VI). This results in an averaged anomalous forcing of -200 W m^{-2}, equivalent to experiment III. In the last experiment with anomalous heat flux forcing, the maximum amplitude of the anomalous forcing is changed such that the anomalous wintertime cooling equals the anomalous heat loss derived from the COADS dataset (Woodruff et al. 1987) (experiment VII). The data are obtained from sensible and latent heat fluxes in January, February, and March in the region between 26° and 42°N, 80° and 30°W (see Fig. 3) in the period from 1954 to 1978. With this experiment we examine whether changes in potential vorticity of the observed amplitude can be generated in the model with anomalous heat losses of the observed amplitude. The pattern shown in Fig. 2c is used to depict the spatial scale of the anomalies.

Also, anomalous wind forcing is applied corresponding to a wind of 2 m s^{-1} (see Fig. 2d). Like the anomalous heat flux experiments this forcing is applied for 1 year (experiment VIII) and for ten years (experiment IX). Finally an experiment with ten years of both anomalous heat flux forcing and anomalous wind forcing has been performed (experiment X).

3. Control run

After initial testing and adjusting parameters in the model, the model was spun up from rest, until it reached a thermodynamical equilibrium after about 1000 years. In this way mode water could form independent of the initial thickness distribution. After the spinup the residual annual diapycnal mass flux into mode water was 7 $\times$ 10^{-4} Sv. At the end a climatology of the model solution was made from the last 20 years of the spinup. First, some basic features of that solution are presented. Also the basic results of the water mass formation are shown. Specific attention is paid to the 18°C layer, which is the model's mode water layer. The results in the next section are mainly based on monthly mean averages.

a. Basic features of the model solution

The annual mean barotropic streamfunction of the model is shown in Fig. 4. The large, anticyclonic sub-

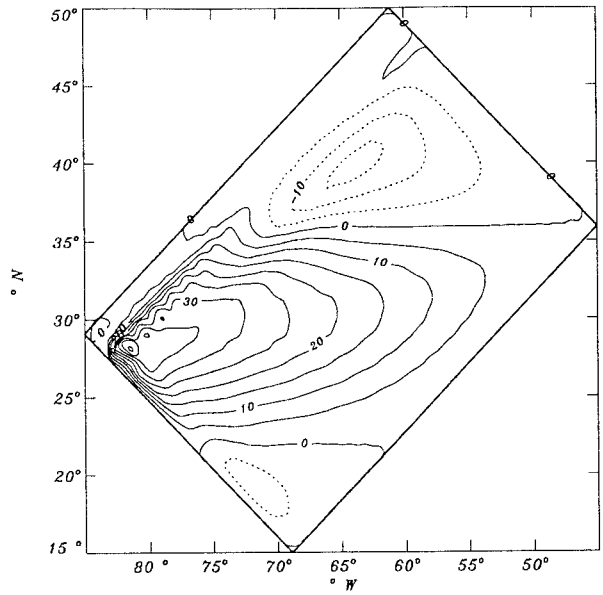

FIG. 4. Annual mean barotropic streamfunction in Sverdrups ($\equiv 10^6$ m^3 s^{-1}).

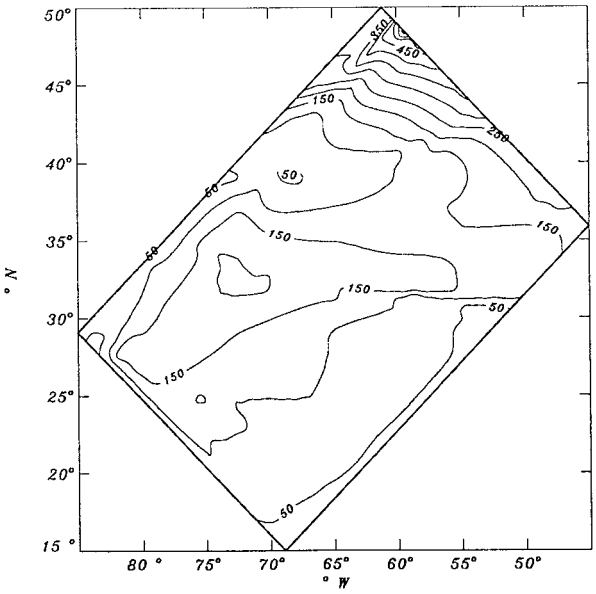

FIG. 5. Monthly mean mixed layer thickness (m) in March.

tropical gyre and the weaker, cyclonic subpolar gyre is consistent with the applied forcing and the basin geometry. An intense western boundary current, which has a small overshoot, is present. The topography, the mixed layer model, and a high resolution can cause an unrealistic overshoot in this model (see Drijfhout 1994a; Drijfhout and Walsteijn 1998). The overshoot did not affect the formation region of mode water. Water leaving the western boundary current recirculates through the large subtropical gyre with transports up to 47 Sv. There is no sign of a tight recirculation near the outflow of the western boundary current. Such a recirculation appears only when the model allows for eddies (e.g., Drijfhout 1994a,b).

An important feature of the ocean model is the mixed layer depth in March. It is crucial to capture the deep mixed layers in the Gulf Stream extension. In this region the mixed layer depth exhibits a large seasonal cycle causing large amounts of well-mixed water to leave the mixed layer and enter the thermocline. This process, combined with the rapid movement of the outcrops, is the reason for the existence of mode water. In section 3b we will look into this process in more detail. In Fig. 5 the thick mixed layers in the Gulf Stream extension are visible. Note the sharp gradient on the eastern side of the subtropical gyre at 32°N. This region will turn out to be important for the formation of mode water. The simulated mixed layer depths are comparable with data obtained from observations (e.g., Marshall et al. 1993). The maximum mixed layer depth in the Gulf Stream region was 220 m in March, which is shallower than the observed maximum of 300 m. The position of this maximum is too far to the west (34°N, 70°W) compared to the observations (39°N, 40°W). This is due to the small basin; the maximum is at the right position with respect to the zonal extension of the subtropical gyre. The general features, especially the broad band of deep mixed layers along the northern boundary of the subtropical gyre are well simulated. Deep mixed layers are found in the north, also consistent with observations. In the summer, in the entire subtropical gyre the mixed layer thickness is less than 50 m, except for a region near the western boundary current where advection of warm water causes a heat loss at the surface, which sets the stage for entrainment, for almost the whole year.

As the objective of this study is to investigate mode water variability, mode water must be well represented in the model solution. In the model the 18°C layer is defined as the mode water layer. A cross section from southwest to northeast is shown in Fig. 6a. The cross section has been taken in June, when most detrainment has taken place. The figure displays the stack of isopycnic layers with the mixed layer on top. The 18°C layer is the thickest subsurface layer corresponding to a potential vorticity minimum, leaving mode water as a dominant feature in our model solution. Also, the typical bowl shape of the thermocline in the subtropical gyre is evident. Horizontally, 18°C Water covers almost the whole subtropical gyre (Fig. 6b) with a maximum thickness of 180 m in the center of the gyre. Furthermore, it exhibits a large seasonal cycle. This is most clearly displayed in the mass fluxes into the different layers as presented in the next section. The 14° and 10°C layers form the thermocline, whereas the 6° and 2°C layers form the deep ocean.

b. Water mass formation

Mode water formation is the result of wintertime cooling followed by springtime warming of the mixed layer

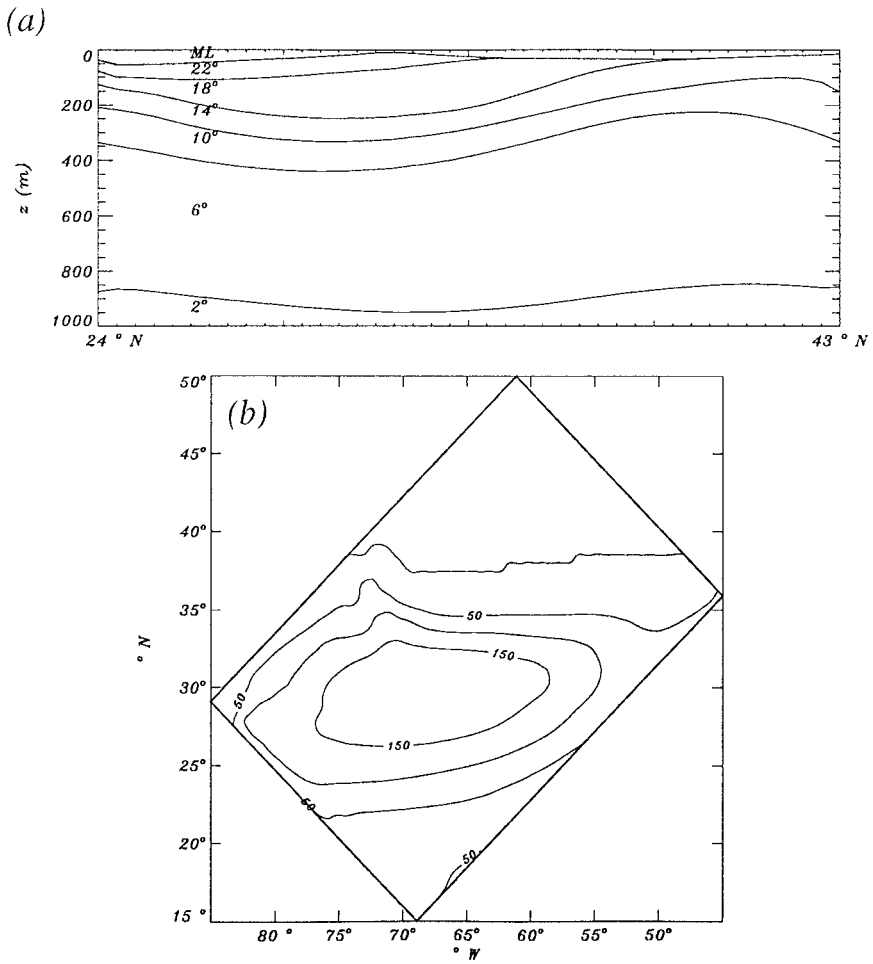

FIG. 6. (a) Cross section from southwest to northeast at maximum mode water thickness in June. (b) Monthly mean thickness (m) of mode water in June.

(Worthington 1959). In the model, the processes by which a specific layer receives or loses water are detrainment from the mixed layer or entrainment into the mixed layer, diapycnal diffusion, and convective adjustment. Consistent with the model formulation these exchanges of water can be explicitly calculated. In the model, the mass flux between the mixed layer and the underlying isopycnal layers is determined by the mixed layer algorithm (see Bleck et al. 1989) and the convective adjustment algorithm. In the latter algorithm an isopycnal layer is mixed into the mixed layer if the stratification becomes unstable, that is, when the mixed layer density is higher than the density of the underlying isopycnal layer. We keep up with these mass fluxes during the integration and calculate directly the subduction. This method is used to determine subduction instead of using a kinematic method (Marshall et al. 1993) or a heat and freshwater flux-based method (Speer and Tziperman 1992). In Figs. 7–9 net mass fluxes (or subduction) are shown. In the present model, the net mass flux into mode water is almost equal to mass flux from and into the mixed layer.

In Fig. 7 the horizontal distribution of the net mass flux in February and May into the mode water layer is shown, when the warming of the surface causes the mixed layer to detrain and leave well-mixed water in the thermocline. This process starts at the northeastern side of the gyre. During spring the region of net monthly subduction shifts to the west. After the month of May mode water formation stops. Mode water formation starts in the east due to the difference in seasonal cycle between the eastern part and the western part of the gyre. The outcrops (not shown) in late winter are deflected to the south on the eastern side of the gyre. In spring they move rapidly to the north, responding to the seasonal cycle in the forcing and cause large heat gain in the mixed layer. On the western side, advection of warm water in the western boundary current dominates, which results in a small seasonal cycle in the position of the outcrops. As the outcrops get more zonal in the

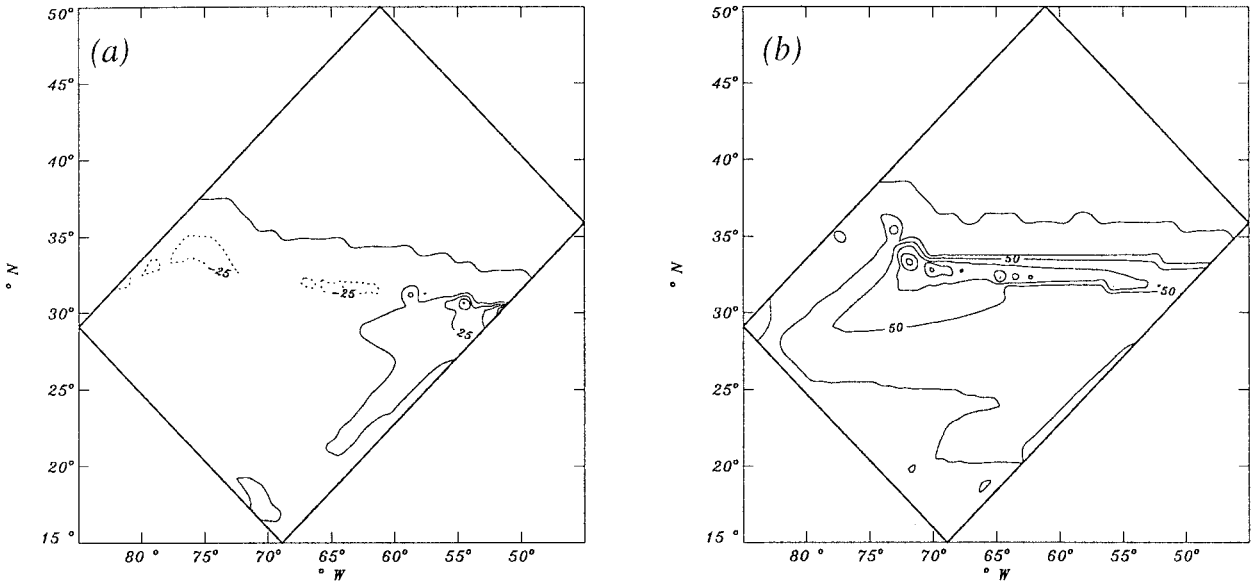

FIG. 7. Horizontal distribution of monthly subduction (m mo^{-1}) for the mode water layer in (a) February and (b) May.

summer the mixed layer ceases to lose heat (because the apparent temperature is zonal as well) and the formation process stops.

The amount of water that ultimately leaves the mixed layer after one annual cycle, the annual subduction, is shown in Fig. 8. A broad band of subduction is visible, with subduction rates up to 200 m yr^{-1} leaving the mixed layer and entering mode water. The band of subduction covers the region of northward movement of the mode water outcrop. This movement is due to warming of the ocean in spring, which sets the stage for detrainment or subduction. When the outcrop moves northward, locally 18°C Water is formed at the outcrop. As a result, the subduction pattern of the spring months can be recognized in the annual subduction pattern.

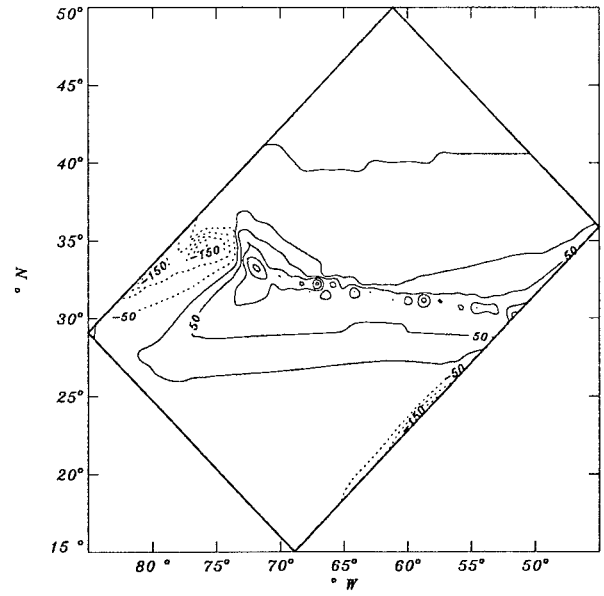

FIG. 8. Horizontal distribution of annual subduction (m yr^{-1}) for the mode water layer.

The amount of water entering the mode water agrees reasonably well with results from other models (Marsh and New 1996; Williams et al. 1995) and observations (Marshall et al. 1993). The mode water layer does not inflate, so there must be regions where the layer loses mass. These regions (indicated by the negative values in Fig. 8) are the western boundary current region where the water is warm enough for cooling-driven entrainment to persist for most of the year and the eastern boundary region where upwelling occurs.

The basin-integrated mass flux for the mixed layer and the mode water layer is shown in Fig. 9. The mixed layer loses large amounts of water during a short period in spring, like in the Cartesian OGCM used by Williams et al. (1995). The entrainment during the rest of the year is a much slower process. Most of the subducted water enters the mode water layer, which is the best ventilated layer in the model in terms of mass flux (the 26°C layer disappears completely in winter and is formed again in spring, being the best ventilated layer in terms of renewal time). At first sight, the monthly subduction seems to be surprisingly large, but due to the short subduction period the annual subduction is even less than observed. This is demonstrated in Fig. 10, where the annual subduction per ventilated layer is displayed (note that only the positive mass fluxes are taken into account, see Fig. 8). It is evident that the 18°C layer is the best ventilated layer in our model. Note also that the 6°C layer is rather well ventilated, being the model equivalent of Labrador Sea Water. The subduction rate, 5.0 Sv, is small compared to observations (e.g., 14 Sv by

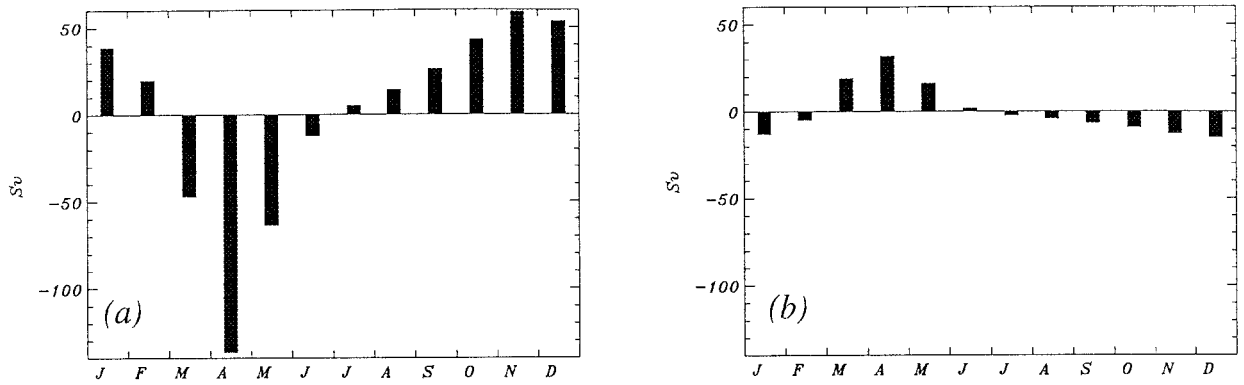

FIG. 9. Seasonal cycle in basin-integrated monthly subduction in Sverdrups for (a) the mixed layer and (b) the mode water layer.

Speer and Tziperman 1992). The reason that subduction is underrated in our model is the small domain of the model. Dividing the annual mean volume of the layer by the annual subduction, one derives the renewal time. For the mode water layer this results in 5 yr, which is fairly short but reasonable. Qiu and Huang (1995) report a renewal time of 18 yr for water in the sigma-theta range of 26.4–26.6 (mode water is observed at the sigma-theta 26.5 isopycnal), while Jenkins (1982) estimated the renewal time for water of sigma-theta 26.5 to vary between extremes of 2.5 yr in the mid-1960s and 5 yr in the early 1960s and mid-1970s.

A different view of the ventilation pattern is obtained by studying the horizontal distribution of the age tracer in the mode water layer (Fig. 11). The three regions defined by Luyten et al. (1983) can be distinguished. A broad, well-ventilated tongue of relatively young water follows the path of the recirculation of the subtropical gyre. This is the ventilated region. As already evident from the monthly subduction, ventilation starts on the northeastern side of the gyre, indicated by the youngest ages. In the southeastern corner the oldest water is found. This is the model equivalent of the badly ventilated shadow zone. On the northern side a small recirculation zone, the pool region, is visible, which was not evident in the barotropic streamfunction. In this region homogenization of potential vorticity can take place according to the theory of Rhines and Young (1982). With the present model configuration this cannot be an important process for mode water variability because the homogenized region is very small compared to the ventilated region. Mode water in the model can be classified as a well-ventilated layer according to the theory of Luyten et al. (1983).

The time for a parcel to cross the subtropical region from the ventilation region to the western boundary current region is around 9 yr. The average age of the mode water layer is 5.9 yr. This value is close to the renewal time as obtained from the subduction. Note that discrepancies between age and renewal times obtained from subduction may occur due to a different method of calculation. Subduction is calculated on every time

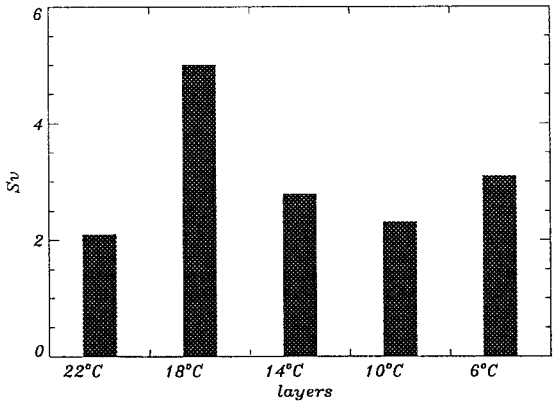

FIG. 10. Annual subduction in Sverdrups for the most ventilated layers.

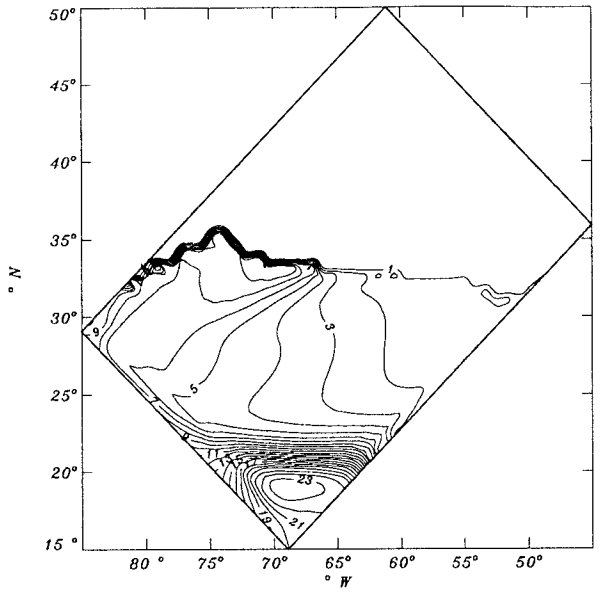

FIG. 11. Horizontal distribution of age tracer (years) in the mode water layer.

step as a one-dimensional process. The water that detrained into mode water in spring can advect away during summer. These processes are reconciled in the age tracer calculation. The age tracer results resemble the results of a model study by Williams et al. (1995). They showed that age on sigma-theta 26.5 is 10 years in the western boundary current region and 30 yr at 10°N at the eastern boundary. In an observational study Jenkins (1988) derived tritium–helium ages of 6 yr in the western boundary current region on the sigma-theta 26.5 isopycnal.

4. Response to anomalous forcings

a. Anomalous heat flux

Seven experiments with anomalous heat flux forcings were conducted (see Table 1). In experiments I and II, the anomalous heat flux patterns of respectively Fig. 2a and Fig. 2b were applied during one winter. The model was then run for another 5 yr with the control forcing. In experiments III, IV, V, VI, and VII the anomalous heat flux pattern of Fig. 2c has been applied. The aim of experiments III and IV is to distinguish the response of mode water formation to a ''sudden'' NAO (experiment III) from a ''gradual'' NAO (experiment IV). In experiments V and VI we study the effect of frequent cold air outbreaks. In experiment V the monthly averaged anomalous forcing vanishes; in experiment VI the monthly averaged heat loss is the same as in experiments III and IV. Finally, in experiment VII a series of anomalous heat fluxes is applied, equal to observational estimates of the years 1954 to 1978.

1) SENSITIVITY TO THE POSITION OF THE ANOMALOUS FORCING (EXPERIMENT I AND II)

In experiment I anomalous cooling in the eastern part of the basin has been applied during one winter (Fig. 2a, Table 1). The mixed layer deepens as a first response to the cold winter (not shown). The anomalous cooling enhances entrainment and deepens the mixed layer at the expense of 18°C Water. The mixed layer is anomalously shallow at the position of the 22°C water outcrop in the summer after the anomalously cold winter. This suggests that more water is subducted in this layer. But, on the contrary, the 22°C layer loses water to the mode water layer in this region, as can be seen in Fig. 12a. A positive anomaly in the thickness distribution is present in the center of the subtropical gyre. At the outcrop of the mode water layer the situation is reversed, water is lost to the 14°C layer demonstrated by the negative thickness anomaly. Apparently, the ocean has cooled as a response to the anomalous heat flux. However, focusing on the mode water layer the response is twofold, that is, losing water in the north to colder layers and receiving water in the south from warmer layers. The same patterns were visible in the distribution of the age tracer. Relatively young water was injected in the center of the mode water layer and into the 14°C layer (not shown).

Both thickness anomalies start to recirculate and attenuate slowly. Figure 12b shows the anomalies one summer later (i.e., more than one year after the anomalous cooling stopped). The velocity of the anomalies was 4.9 cm s^{-1} at 25°N. This is in the range of the baroclinic planetary wave speed if one takes the mean velocity in the gyre ($\sim$ 1.2 cm s^{-1}) into account. In Fig. 12c the thickness anomalies five years after the cold winter is shown. The original anomalies have almost disappeared, but an interesting new feature appears. When the positive thickness anomaly reaches the outflow of the Gulf Stream, a new negative thickness anomaly is formed at 32°N, 60°W. As pointed out by Cox (1987), planetary waves recirculating around the gyre may induce new anomalies when they reach the western boundary current. With the present model resolution this anomaly loses its significance within a year, but it may become more prolonged when the explicit diffusion is reduced and the model allows eddies or when the ocean model is coupled to an atmospheric model. In the latter case the temperature is not restored to a fixed apparent temperature but to a variable apparent temperature that can be influenced by SST anomalies. In that case, the inherent feedback processes may reduce the attenuation of the anomaly.

The original negative thickness anomaly on the eastern side of the gyre can be attenuated due to diapycnal processes or due to stretching (i.e., conservation of potential vorticity). For a fluid column to turn south, it must get thinner and spread to maintain its potential vorticity. If this process is acting in the model, the amplitude of the negative thickness anomaly in the mode water layer must reduce as well. To examine whether the loss of planetary vorticity of the anomaly is thermally compensated we partitioned potential vorticity Q in three terms:

$$Q = \frac{f + q}{h} = \frac{f}{h_*} + \frac{q}{h_*} + \frac{(h_* - h)}{h}\frac{(f + q)}{h_*},$$

where f is the planetary vorticity, q is the relative vorticity, h is the thickness of the layer at the position of the anomaly, and h_* is an arbitrary constant thickness (e.g., the initial thickness).

Figure 13 shows the contribution of the first and the third term to the potential vorticity of the mode water layer following the minimum of the negative thickness anomaly. The curve starts at the time when the anomaly turns south. Before that time it is hard to identify the minimum of the thickness anomaly because the anomaly is still being formed. The path of the negative anomaly is depicted by the contribution of the planetary vorticity to the potential vorticity. This contribution drops slowly, consistent with the movement of the anomaly to the south. The second term is not shown because it is two

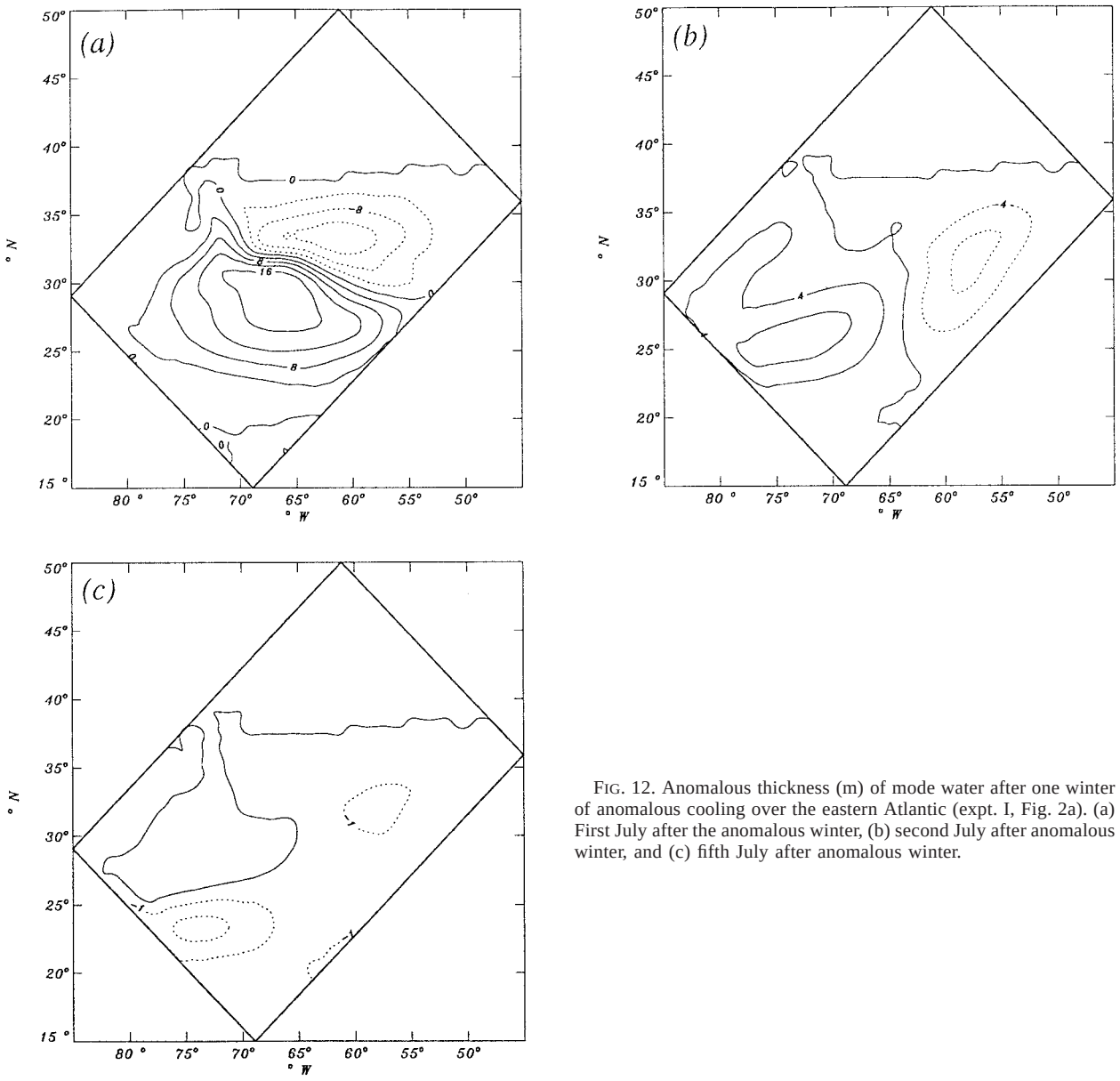

FIG. 12. Anomalous thickness (m) of mode water after one winter of anomalous cooling over the eastern Atlantic (expt. I, Fig. 2a). (a) First July after the anomalous winter, (b) second July after anomalous winter, and (c) fifth July after anomalous winter.

orders of magnitude smaller compared to the other terms. The third term represents the contribution of the change in layer thickness at the position of the anomaly. This contribution drops rapidly at the start of the circulation of the anomaly and then rises slowly (Fig. 13b). The slow rise after month 16 is consistent with the conservation of potential vorticity, compensating for the change in f due to the southward movement. This is confirmed by the tendency of potential vorticity, which is shown in Fig. 13c. Two features remain to be explained: the drop of potential vorticity in the first months and the increase and decrease in the 25th to the 27th month. To elucidate the processes involved in these changes we diagnose the sources of potential vorticity from the mass fluxes associated with the various diapycnal processes. In Fig. 13c only the contribution of entrainment and detrainment to the tendency of potential vorticity in the mode water layer is shown because diffusive processes play a negligible role. Initially, the thickness anomaly is formed and detrainment from the mixed layer acts as a sink for its potential vorticity. After month 16 potential vorticity is almost conserved, apart from a small positive contribution of entrainment that rises slowly toward the winter. In month 25 detrainment reinforces the anomaly. After month 27, potential vorticity is exactly conserved. Apart from a short period in the winter, when mass is exchanged with the mixed layer, potential vorticity in the recirculation is largely conserved.

The positive thickness anomaly is more dominant

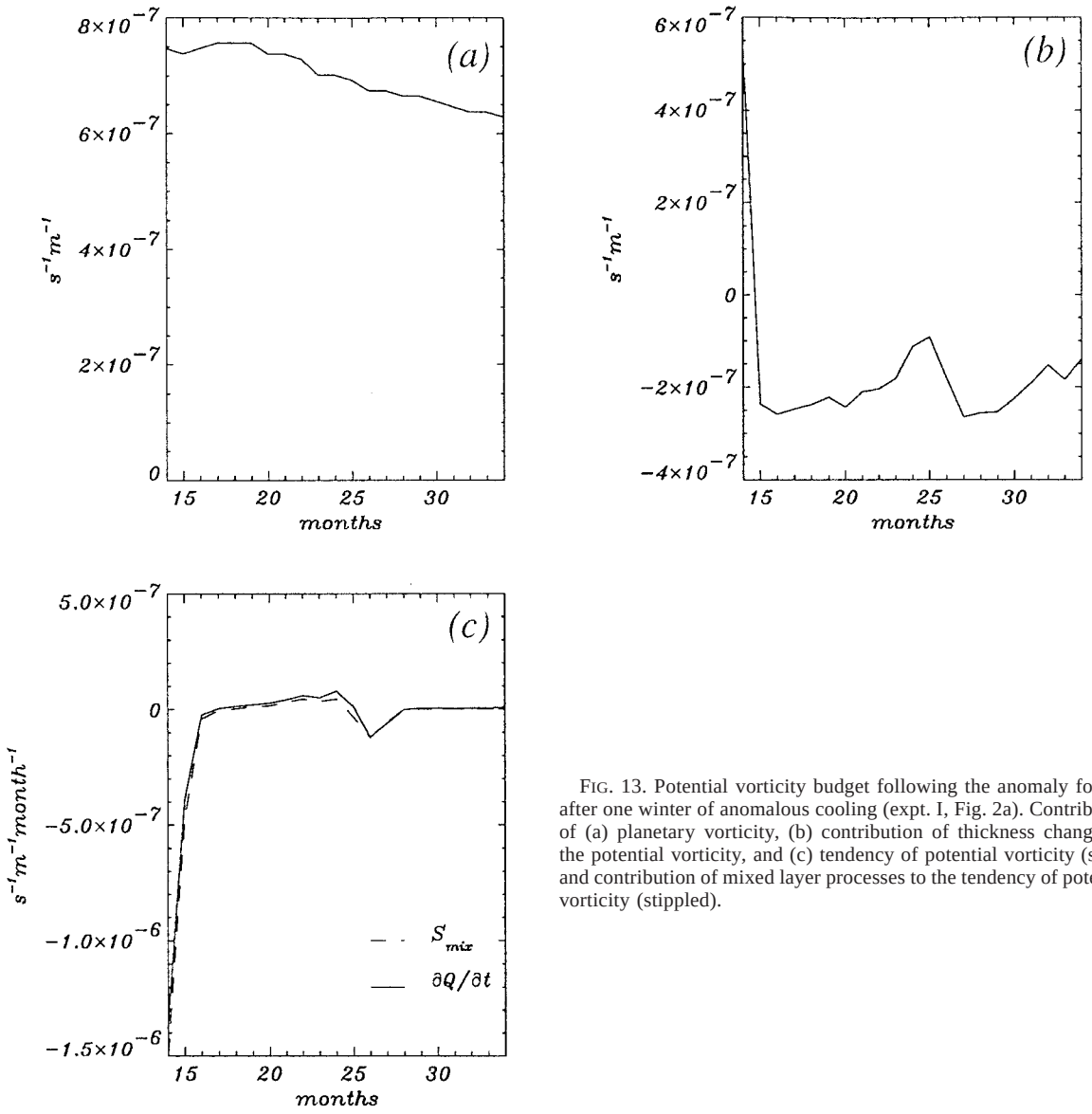

FIG. 13. Potential vorticity budget following the anomaly formed after one winter of anomalous cooling (expt. I, Fig. 2a). Contribution of (a) planetary vorticity, (b) contribution of thickness changes to the potential vorticity, and (c) tendency of potential vorticity (solid) and contribution of mixed layer processes to the tendency of potential vorticity (stippled).

than the negative anomaly when focusing on the total volume of the mode water layer. In this enhanced cooling experiment, the annual subduction into the mode water layer has increased by 0.9 Sv. Comparable results have been presented by Marsh and New (1996).

There is no sign of an anomalous recirculation driven by the cooling, as found by Huang (1990). The maximum increase of the barotropic transport is 0.5 Sv, which is too weak to play a significant role in the evolution of potential vorticity anomalies. The anomalous velocity fields within the layers are geostrophically consistent with the anomaly. The response of the mode water thickness to cooling is twofold (see Fig. 12). Consistent with the pressure changes on the interfaces the flow is anomalously anticyclonic at the position of the positive thickness anomaly. At the position of the negative thickness anomaly the flow is anomalously cyclonic. The lack of a high barotropic pressure south of the outcrop may be attributed to the low horizontal resolution and the high viscous dissipation of the model. Drijfhout (1994b) found that an anticyclonic recirculation driven by cooling was intensified in an eddy-resolving version of the model. Also, the use of a rigid lid might partly be responsible for this. Marsh and New (1996) found a weak intensification of the recirculation induced by cooling in a comparable model as used here, but their model contained a free surface.

Experiment II has been conducted in order to show the sensitivity of mode water variability to the position of the anomalous forcing. The strong cooling in the southwest (see Fig. 2b, Table 1) causes the mixed layer to deepen as a first response. Comparing to experiment

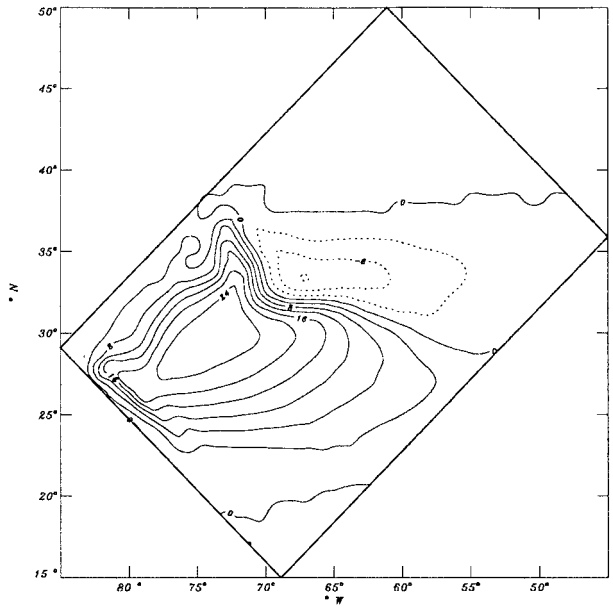

FIG. 14. Anomalous thickness (m) of mode water in July after anomalous winter with cooling over the southwestern Atlantic (expt. II, Fig. 2b).

I, the positive thickness anomaly in mode water is more dominant now. This shows the sensitivity of mode water formation to the position of the forcing. On the western side of the subtropical gyre large volumes of water are exchanged between the 22°C layer and the 18°C layer (Fig. 14). As in the first experiment, the positive thickness anomaly hardly recirculates.

The positive thickness anomaly is studied in more detail in order to examine the processes involved in the formation and the attenuation of this anomaly. A time series of the potential vorticity, $(f + q)/h$, in the center of the recirculation at 25°N, 76°W is shown in Fig. 15a. This point is chosen to compare with TR's time series of potential vorticity at Panulirus Station because of the comparable position in the recirculation of the gyre. In Fig. 15 the cooling starts in the 19th month, at the end of the second year, and stops after the 30th month. The potential vorticity in the first 12 months is derived from the control run.

The seasonal cycle is evident in the increase of potential vorticity in the winter months, followed by a decrease during spring. The entrainment of 18°C Water by the mixed layer, induced by cooling at the surface in the fall and winter, is the cause of the rise of potential vorticity in the 18°C layer, while detrainment accounts for the drop during spring. A rapid rise followed by an

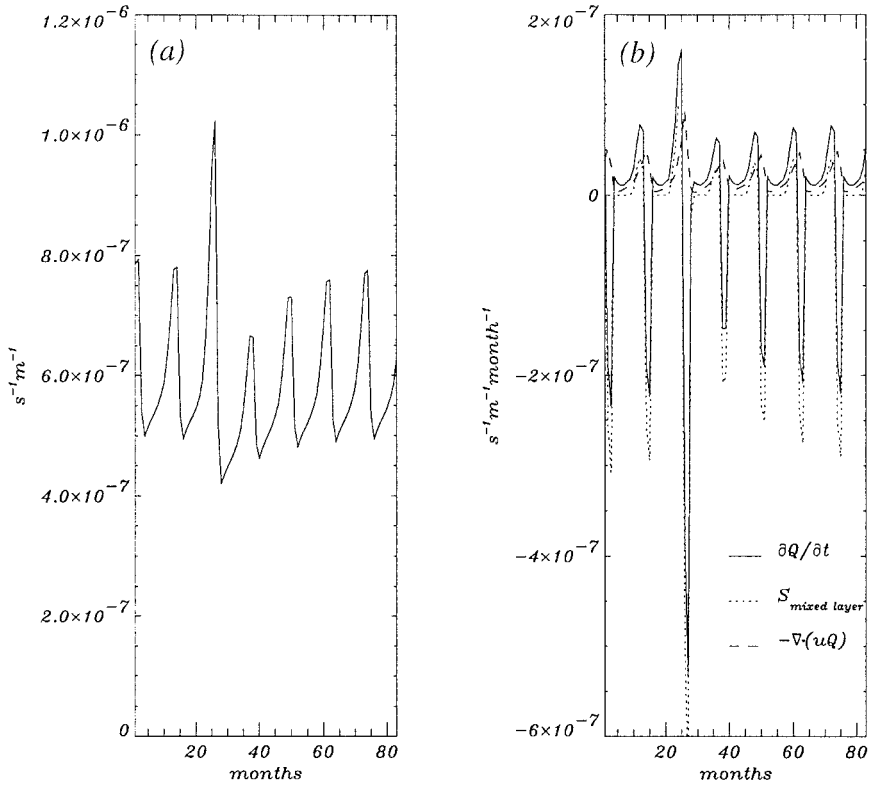

FIG. 15. Time series of (a) the potential vorticity of the mode water layer at 25°N, 76°W and (b) the tendency of potential vorticity, the contribution of mixed layer processes, and the contribution of advection. The second winter, corresponding to the peak in potential vorticity, was anomalously cold (expt. II, Fig. 2b).

even larger drop in potential vorticity is evident after the cold winter at the end the second year and in the first months of the third year. To understand the potential vorticity evolution we examine the different terms of the potential vorticity equation. The equation reads

$$\frac{\partial Q}{\partial t} = -\nabla\cdot(Q\mathbf{u}) + \mathcal{F} + \mathcal{S},$$

where Q is the potential vorticity $(f + q)/h$, $\mathbf{u} = (u, v)$ the horizontal velocity, $\mathcal{F}$ is the contribution of the viscous forces, and $\mathcal{S}$ represents a source term, determined by entrainment and detrainment, diapycnal diffusion, and convective adjustment. The contributions to the potential vorticity budget induced by these processes are diagnosed from the mass fluxes during the integration. Figure 15b shows the contribution of entrainment and detrainment and advection to the potential vorticity budget, as well as the tendency of potential vorticity itself. At Panulirus Station the budget is almost completely controlled by entrainment and detrainment. Advection acts to increase the potential vorticity and closes the budget. The positive contribution of advection is in contrast to the hypothesis of TR. They assumed that negative potential vorticity anomalies are advected from the formation region to Panulirus Station. Note the time lag between the maximum in the contribution of entrainment and the maximum in the contribution of advection. This suggests that the water column was subject to entrainment before being advected to the model's Panulirus Station. The contributions of diapycnal diffusion, convection, and horizontal viscosity are negligible.

The anomalous cooling starting at the end of the second year enhances the entrainment in the winter, which results in an anomalous rise of potential vorticity in the mode water layer. In the spring after the anomalous winter, enhanced detrainment rates induce a negative potential vorticity anomaly in the mode water layer. The depth to which the mixed layer will detrain is determined by the Monin–Obukhov length, $L = u_*^3/(-\kappa B_0)$. The enhanced detrainment means that the Monin–Obukhov length has become smaller. This must be due to a larger buoyancy flux B_0 because the wind stress was not changed during this experiment. The anomalously cold winter generated low SSTs, which is associated with a large B_0 due to the restoring term in the heat flux forcing (see section 2b). After a period of anomalous forcing a more stable stratification remains. While the SST turns back to climatology on the restoring timescale, the stable stratification remains after the anomalous forcing stopped. Consequently, the entrainment rate is reduced at the end of the third year and there is less water to detrain at the start of the fourth year. The result is that the negative potential vorticity anomaly persists in the mode water layer after the anomalous forcing has stopped. A cycle of anomalously weak entrainment and detrainment persists for about 5 yr, which is the timescale for the stratification to restore after an anomalous cooling event. (This timescale appeared to be robust. An experiment with a coupling half as strong between the atmosphere and the ocean yielded the same timescale. However, the amplitude of the generated potential vorticity anomaly was larger. This was due to the fact that temperature anomalies could last longer in the mixed layer because of the longer restoring timescale. Consequently, entrainment and detrainment was enhanced compared to experiment II.) The reduced detrainment rate after the anomalous forcing stopped is also demonstrated by the annual subduction, which is 0.4 Sv less than normal in the fourth year. Diapycnal diffusion and lateral viscosity appear to be unimportant for the potential vorticity evolution in the mode water layer.

The amplitude of the large drop in potential vorticity after the anomalous winter resembles the results of TR and Marsh and New (1996). Using the same units as TR, a drop in potential vorticity of 70×10^{-14} s^{-1} cm^{-1} is found, which is somewhat larger than in TR. In section 4a(2) results of experiments with prolonged anomalies are described.

2) Sensitivity to timescales of the forcing (experiment III, IV, V, and VI)

In experiments III, IV, V, and VI the anomalous heat flux forcing pattern shown in Fig. 2c is applied. With this pattern of anomalous forcing the anomalously low potential vorticity of the mode water layer as well as the positive potential vorticity anomaly on the eastern side of the gyre is retained.

In experiment III, the anomalous cooling is applied for ten consecutive winters in the center of the basin, with a maximum amplitude of -200 W m^{-2} each winter (Fig. 2c, Table 1). A large positive and negative thickness anomaly is generated (Fig. 16). In contrast to experiments I and II, the negative anomaly does not recirculate. Every winter enhanced entrainment followed by enhanced detrainment induces new thickness anomalies in the mode water layer. After the ten anomalous winters the evolution of thickness anomalies follows the same course as the anomalies in experiments I and II.

Again, a time series of potential vorticity at the model's Panulirus Station is presented (Fig. 17a). The cooling starts in the 19th month and lasts for 10 years. A prolonged negative potential vorticity anomaly is evident in the time series. During the 10 years of anomalous forcing the potential vorticity anomaly persists in the mode water layer. The formation and the attenuation of the anomaly can be attributed to the same entrainment and detrainment processes as in experiment II [see section 4a(1)]. The low potential vorticity in the winter after the anomalous forcing stopped seems remarkable, but the same minimum is visible in Fig. 15a. The drop is induced by the reduced entrainment, which is caused by the anomalously stable stratification created by the anomalous forcing. The amplitude of the change in po-

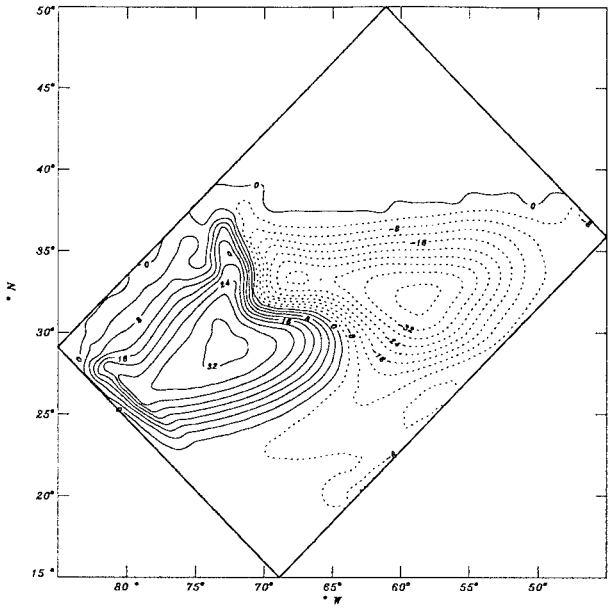

FIG. 16. Anomalous thickness (m) of the mode water layer in July of year 9 in the experiment with ten consecutive cold winters (expt. III, Fig. 2c).

tential vorticity is larger than the amplitude in experiment II. It is obvious that a regime shift in the atmospheric forcing, which is mimicked in this experiment, can induce a prolonged potential vorticity anomaly with a timescale comparable to the timescale found by TR. However, the amplitude of the change in potential vorticity is 80×10^{-14} s^{-1} cm^{-1}, compared to an observed change of approximately 50×10^{-14} s^{-1} cm^{-1}. This discrepancy is due to the very strong cooling. To obtain a change of potential vorticity of the observed amplitude, the maximum heat loss must be at least 100 W m^{-2}. Although such anomalous cooling occurred in some years in the 1950s and 1960s, the average heat loss was not that high [see section 4a(3)].

In Fig. 17b the evolution of potential vorticity resulting from experiment IV is presented. In this experiment a gradual variation in the maximum of anomalous wintertime heat loss is applied. Each winter the anomalous heat flux forcing is switched on. The maximum amplitude of the forcing varies sinusoidally with a period of 20 yr (Fig. 2c, Table 1). The negative potential vorticity anomaly forms more gradually in this experiment. In the second decade the anomalous heat flux forcing is positive and slowly a positive potential vorticity anomaly is formed. During the anomalously warm winters the entrainment rates are reduced due to the reduced heat loss. Consequently, the higher SSTs induce a reduction in the detrainment rates as well. This experiment shows that in the model a gradual change in the forcing cannot account for the observed sudden shift from ''normal'' mode water to more denser and colder mode water as observed in the early 1960s by TR.

In experiment V the average anomalous forcing is zero, but each month there is a short period of strong anomalous cooling (a maximum amplitude of -800 W m^{-2} during 5 days) compensated by a longer period of anomalous warming, yielding no average anomalous forcing (Fig. 2c, Table 1). This type of forcing did not affect the mode water layer strongly. Compared to the control run, potential vorticity reduces slightly (Fig. 17c). The amplitude of the generated thickness anomaly in mode water was 4 m in July.

In experiment VI the outbreaks are followed by a longer period of slightly anomalous cooling resulting in an anomalous heat loss of 200 W m^{-2}, which is equal to experiment III (Fig. 2c, Table 1). The aim of this experiment is to compare the response to frequent strong outbreaks with the response to a more prolonged weak cooling. A strong and prolonged potential vorticity anomaly is generated (Fig. 17d). The maximum positive thickness anomaly in July was 48 m, compared to 32 m in experiment III. The strong anomaly is formed by the same processes as described in section 4a(1). Clearly, the effect of outbreaks of very cold air on the mode water formation increases when the period of ''normal'' conditions shows more cooling.

3) RESPONSE TO OBSERVED ANOMALOUS COOLING (EXPERIMENT VII)

In experiment VII anomalous heat fluxes of the observed amplitude are applied (Fig. 2c, Table 1). The heat losses are derived from historical data as described in section 2b. The spatial and time averaged anomalous heat losses are shown in Fig. 18a. A regime shift in the observed heat fluxes is not present, although the 1970s are notably warmer than the 1950s and the 1960s. The response to anomalous heat fluxes of the observed amplitude is shown in Fig. 18b. Focusing on the yearly minimum in potential vorticity, a prolonged negative vorticity anomaly is formed in the model's mode water in the early 1960s. The anomaly persists for more than 10 yr. In 1972 the potential vorticity rises and remains high. Similar changes have been observed by TR at Panulirus Station. In their time series the negative potential vorticity anomaly forms some years later than in our model, for which the attenuation of the anomaly takes place in exactly the same years. Also, the amplitude of the potential vorticity changes in the model is comparable to the observations. The difference in potential vorticity between the period in the 1950s and the 1960s is 40×10^{-14} s^{-1} cm^{-1}. In the observations, as well as in the model, the rise in potential vorticity in the early 1970s is larger. In the model the rise is 60×10^{-14} s^{-1} cm^{-1}. The good agreement between the model results and the observations suggests that a few very cold winters within a longer period in the 1960s are responsible for the anomalously low potential vorticity during those years. The anomaly does not attenuate because one interrupting year of warming (e.g., 1967) is a too short period to attenuate the anomaly. The per-

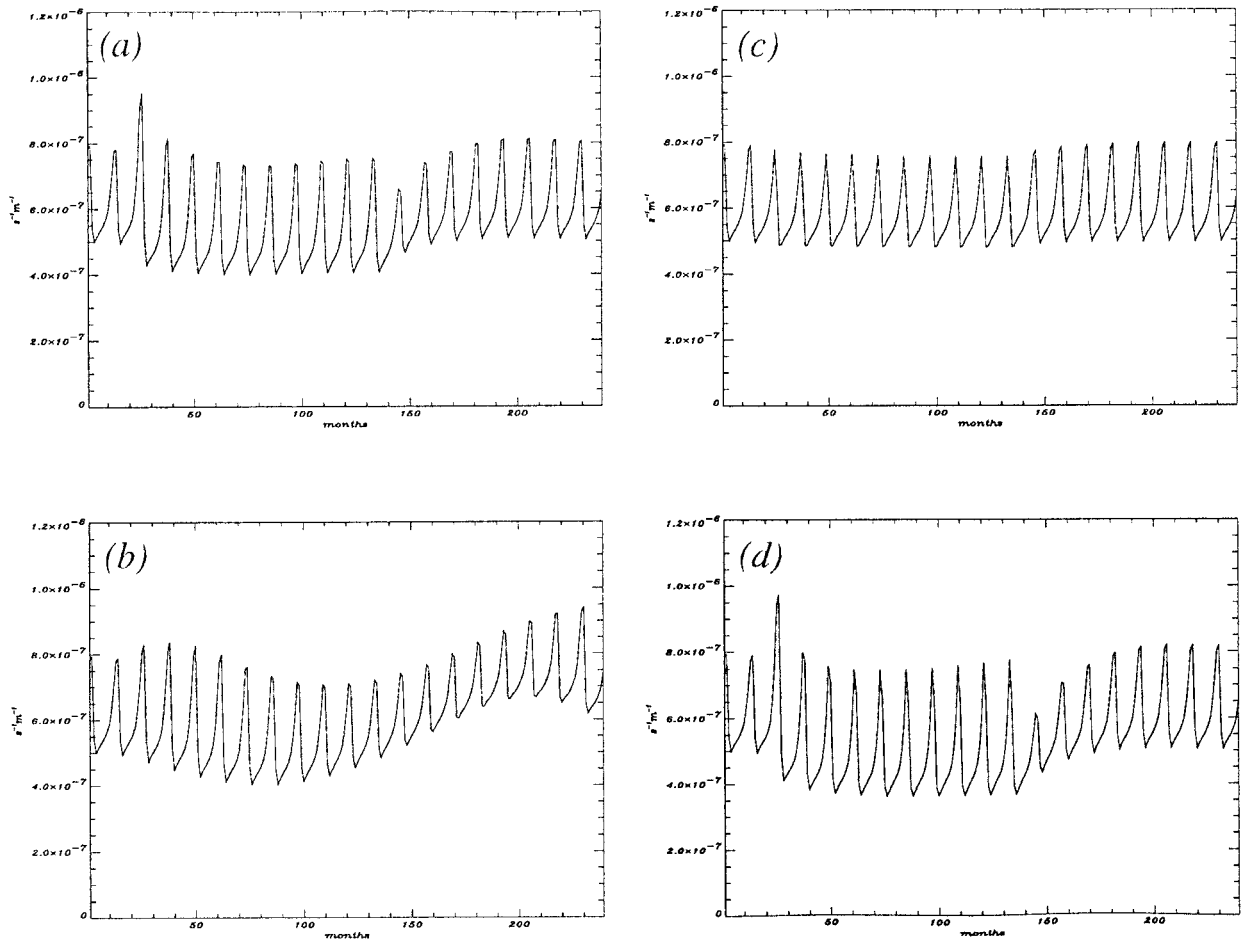

FIG. 17. Time series of potential vorticity of the mode water layer at 25°N, 76°W in (a) expt. III (10 cold winters), (b) expt. IV (maximum amplitude varies sinusoidally with a 20-yr period), (c) expt. V (cold air outbreaks, but no average cooling), and (d) expt. VI (cold air outbreaks with average cooling of 200 W m^{-2})

sistence of the anomalously stable stratification that weakens entrainment and detrainment is the cause of the ''storage mechanism,'' already proposed by Jenkins (1982). When several warm years succeeded each other in the 1970s, the anomaly could be attenuated (see discussion in §5).

b. Anomalous wind stress

In experiment VIII one winter of anomalous wind forcing is applied as displayed in Fig. 2d (Table 1). The model was then run for another 5 yr with the control forcing. The anomalously strong winds in the winter season put more turbulent kinetic energy into the mixed layer. The consequence is an overall thickening of the mixed layer, except for regions in the north where anomalous advection of warm water suppresses entrainment. The outcrops of the different layers are visible in the anomalous thickness field of the mixed layer (not shown). This is an artifact of layer models caused by the differences between the density of the upper layer and the layer beneath the mixed layer (due to the discretization of the vertical coordinate the outcrop is a band of finite width: on top of the isothermal mode water layer the mixed layer temperature changes from 18° to 22°C; consequently the fluid column is less stable on the northern side of the outcrop than on the southern side of the outcrop). As a first response the mode water layer loses water to the mixed layer. The barotropic streamfunction is enhanced by 16 Sv.

After the winter with anomalously strong winds, thickness anomalies start to propagate. Adjustment by long baroclinic Rossby waves (or thickness anomalies) takes place. The thickness anomalies radiate from the eastern boundary (Fig. 19a). In Fig. 19b the same thickness anomalies can be recognized 1 yr later. The anomalies have propagated to the west along two paths. One path follows the recirculation of the subtropical gyre; the other path follows the outcrop of mode water. The thickness anomalies formed around 34°N, 70°W are strongly affected by mixed layer processes. Initially, the negative thickness anomaly at 33°N, 73°W (see Fig. 19a)

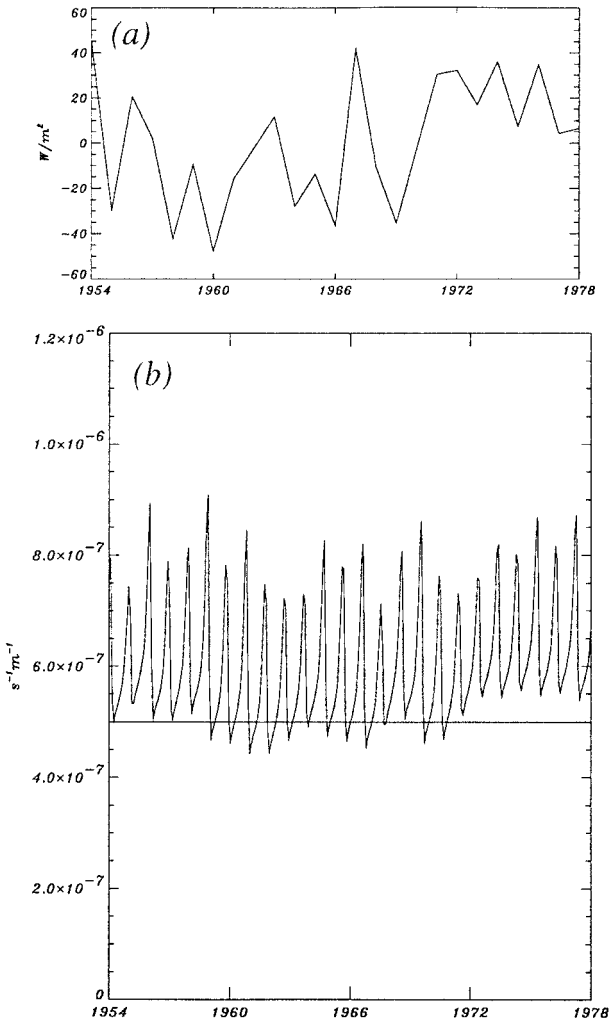

FIG. 18. (a) Anomalous heat flux derived from historical data and (b) time series of potential vorticity of the mode water layer at 25°N, 76°W in expt. VII (straight line is the potential vorticity minimum derived from the control run).

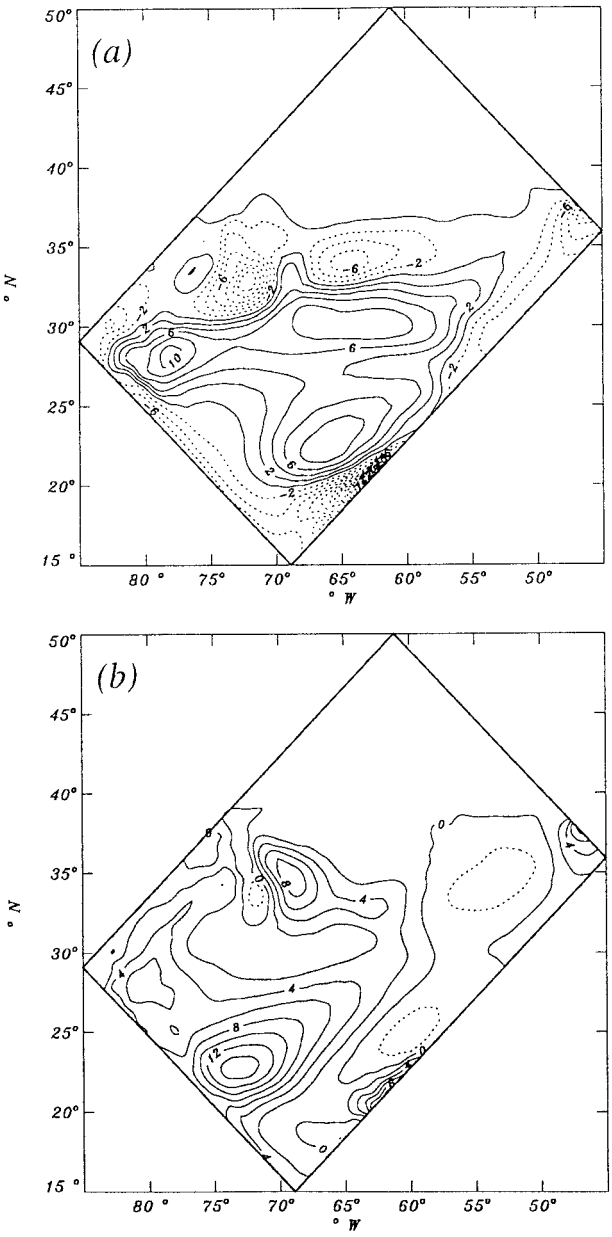

FIG. 19. Anomalous thickness (m) of mode water in experiment with one winter with anomalous wind stress (expt. VIII, Fig. 2d). (a) First July after anomalous winter and (b) second July after anomalous winter.

is formed by anomalous entrainment. It is advected by the mean flow to the east afterward (see also Fig. 20a). In general, thickness anomalies in the mode water layer are compensated by thickness anomalies of the opposite sign in the mixed layer. In the next spring, when detrainment takes place, positive thickness anomalies are generated to the northeast and northwest of the original negative thickness anomaly. Thereafter, adjustment of small positive vortices and the larger negative vortex by mixing and advection takes place, resulting in a near cancellation of the positive and negative thickness anomalies (see Figs. 19b and 20a at 34°N, 74°W). During summer when the detrainment stops, the remnant of the negative anomaly advects away and diffuses slowly. The next spring this process starts again, but the anomalies are weaker (see Fig. 20a).

The center of the gyre is relatively unaffected compared to the anomalous heat flux experiments. The maximum potential vorticity anomaly at Panulirus was 8×10^{-14} cm^{-1} s^{-1}, while TR observed potential vorticity changes of 50×10^{-14} cm^{-1} s^{-1}. This amplitude of the potential vorticity anomalies is much smaller than when generated by anomalous cooling. The generated anomalies can be identified as planetary waves. The time–longitude diagrams in Fig. 20 show the propagation of the thickness anomalies at two latitudes. The westward propagation of the anomalies at 25°N is evident in Fig. 20b. The amplitudes of the newly formed anomalies

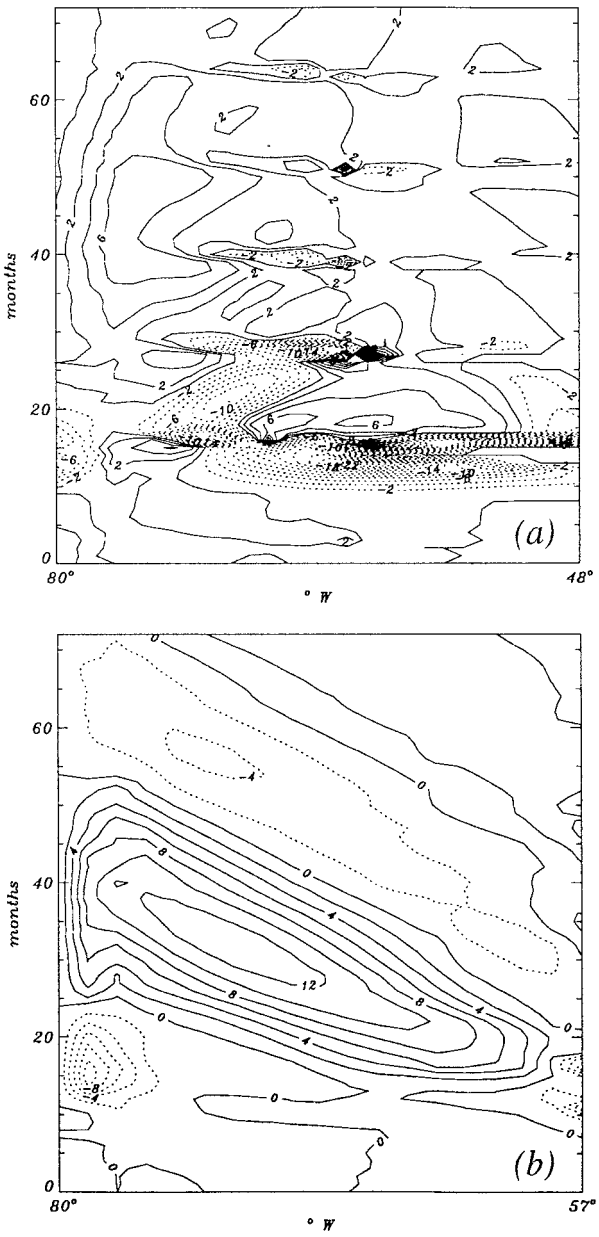

FIG. 20. Time–longitude diagrams of thickness anomalies (m) in experiment with one winter with anomalous wind stress (expt. VIII, Fig. 2d) at (a) 34°N and (b) 25°N.

become progressively smaller as the ocean adjusts toward the control state again. The mean velocity of the anomalies is 5.3 cm s^{-1}. Taking into account the mean velocity in the recirculation of the gyre, the phase velocity is 4.1 cm s^{-1}, which is close to the theoretical phase velocity of the first baroclinic mode derived from the stratification at the position of the anomaly (Pedlosky 1987), which is 4.4 cm s^{-1}. Also the vertical structure of the anomalies (not shown) suggests that the anomalies are primarily first baroclinic modes. The wavelength of the anomalies is approximately 2100 km.

At 34°N the anomalies propagate in a much more complicated way (Fig. 20a). The large negative thickness anomaly that appears in the 10th month depicts the enhanced entrainment of mode water by the mixed layer induced by the strong winds. After the winter with anomalously strong winds, two negative thickness anomalies emerge. The negative anomaly formed at 73°W starts to propagate to the east, carried by the mean flow. Each following spring, it reappears at the same position (~68°W), but with a smaller amplitude. As explained before, detrainment and advection play a role in the evolution of this anomaly. The anomaly formed at 55°W is able to propagate westward without interaction with the mixed layer, although its propagation is slow caused by the eastward mean flow.

The results of an experiment with 10 years of anomalous wind stress forcing (experiment IX) did not reveal new features. Adjustment took place by radiating planetary waves and after about 5 yr the ocean had adjusted to the new forcing. After the anomalous forcing stopped, the ocean adjusted again to the control state within 5 yr. Again, the center of the gyre was relatively unaffected.

Finally we mention that subduction into mode water is enhanced by the strong winds due to the enhanced entrainment. The effect is quite strong: 6.25 Sv is subducted into the mode water compared to 5.0 Sv in the control run and 6.9 Sv in experiment I.

As described in section 3b we also conducted an experiment with both anomalous heat flux and anomalous wind forcing (experiment X). The results of this experiment did not show a strong interaction between the anomalies formed by the different anomalous forcings. The dipole in the anomalous thickness distribution induced by the anomalous cooling was most dominant with recirculating thickness anomalies induced by the anomalous wind superimposed on it.

5. Discussion

In this study the geometry and the forcing of the model are deliberately kept simple. This allowed us to perform a series of sensitivity experiments and to focus on processes. However, we refer frequently to observations, and one might question whether this is appropriate. First, we will discuss to what extent the idealizations might affect the results.

In the model, mode water is formed at the location of the Panulirus Station, where it interacts with the mixed layer during the winter. In reality, mode water is advected toward Panulirus (TR; McCartney 1982). In winter, a less dense layer can be found in between the mode water layer and the mixed layer base. If local air–sea interaction mechanisms drive mode water variability, a time lag between the forcing and response at Panulirus will be observed. Due to the finite vertical resolution this warmer layer and a time lag between the forcing and response are absent in the model. Indeed,

in the 1960s the negative potential vorticity anomaly starts too early in the model compared to the observations. However, apart from the time lag, the finite vertical resolution did not appear to affect the results further.

A comparison of experiments III (prolonged weak cooling) and VI (cooling as in III, but in the form of outbreaks) reveals that lower potential vorticity mode water forms under outbreaks. Perhaps this is partly why low potential vorticity is not evident in 1977 of experiment VII. Also, the applied heat flux anomaly in Fig. 18a shows that there was not much cooling in 1977, although the 1976/77 winter along the eastern seaboard was indeed very severe. The region used to average the historical heat fluxes might be too large (extending too far eastward) to capture outbreak cooling, which weakens rapidly with distance offshore. Furthermore, the spatial pattern of the observed variability has been reduced to simple dipole patterns (Fig. 2).

Eddies are not resolved in our model. Eddies will change the subduction patterns and affect the potential vorticity budgets. Williams et al. (1995) report that incorporating eddies enhances tracer transfer into poorly ventilated zones. They will also induce internal variability in the model. However, the response to the anomalous heat flux in the present model is very strong and will not change when resolving eddies. The role of eddies in inducing mode water variability is the subject of a later study.

In the present model, the parameterization of the atmospheric forcing is very simple. The heat flux is parameterized with a restoring boundary condition. A drag relation for parameterizing the heat flux, dependent on the wind speed, will result in larger responses caused by the anomalous wind stress. Also, positive feedback processes can delay the attenuation of anomalies. In a following study we will couple our model to a simple atmospheric model such that air–sea interaction will be better parameterized. With such a model we will be able to investigate the role of coupled modes of instability in generating mode water variability.

A rather simple bulk mixed layer model is used in this study. The Kraus–Turner mixed layer model overestimates the sensitivity to wind stress variations (Martin 1985). If a more sophisticated mixed layer model was used, the response to anomalous wind forcing would even be less. In heating experiments, Martin (1985) found that Kraus–Turner mixed layers produce too shallow mixed layers. This can be attributed to the dependence of the detrainment on the Monin–Obukhov length scale and the Ekman length scale in more complex models. By including a damping term, dependent on the Ekman length scale, in the parameterization of the production of turbulent kinetic energy by the wind stress we tried to solve this problem.

The present model has a very regional character. It is not suited to study the influence of nonlocal mechanisms. A basin-scale model is needed to study the coupling between mode water formation and, for example, the formation of Labrador Sea Water or North Atlantic Deep Water. Also, the Mid-Atlantic Ridge is not included. JEBAR (joint effect of baroclinicity and relief) may play a role in mode water variability. Changing the surface forcing in the vicinity of topography may induce higher-order dynamics in the model.

The model is suited to study the role of local air–sea interaction mechanisms in generating mode water variability. The suite of experiments shows that generic values of anomalous heat flux, as well as anomalous wind stress, can generate variability in mode water formation of the observed magnitude.

The anomalous heat loss cools the ocean but, focusing on water masses, the response is twofold. Mode water loses water to the 14°C layer in the north, but receives water from the 22°C layer in the south. Such a dipole in the anomalous thickness distribution has also been shown by Marsh and New (1996). The relative strength of the thickness anomalies is sensitive to the position of the anomaly with respect to the formation areas of the water masses. In the center of the gyre, mode water always receives water during a cooling event.

The formation of thickness anomalies is a quick process, determined by entrainment and detrainment. These mixed layer processes act on a timescale of the order of days. After the anomalous cooling stops, the thickness anomaly formed in the northeast starts to recirculate, while the anomaly formed in the center of the gyre hardly recirculates. The attenuation of both anomalies can be attributed to different processes. The negative thickness anomaly, formed at the outcrop of mode water, has a wavelike character and propagates to the southwest. The reduction of its amplitude is mainly the result of conservation of potential vorticity. The mixed layer hardly interacts with the anomaly after it is formed, except for a short period in the winter. Progressively deeper layers have less interaction with the mixed layer. Anomalies in the 10°C layer persist very long, but their amplitude is very small (less than 1 m). The attenuation of the thickness anomaly in the center of the gyre is mainly due to entrainment and detrainment processes. Advection is less important and acts to raise the potential vorticity of the mode water. This is in contrast to the hypothesis of TR. They argue that the observed negative vorticity anomalies are advected from the formation region. The role of advection, however, may be very sensitive to details of the model, such as resolution and viscous dissipation. The attenuation of the anomalies is a fairly slow process. This is due to the anomalously stable stratification induced by the cooling. In the model, a typical period of 5 years is needed to remove a positive thickness anomaly in the center of the mode water layer.

Local air–sea interactions in conjunction with entrainment and detrainment processes generate a potential vorticity anomaly in the center of the mode water layer. Therefore, a long multiyear period of anomalous atmospheric conditions can generate mode water anom-

alies of the observed timescale. This is demonstrated by the results of experiment III where cooling is applied for a long period. A sudden change in the potential vorticity of the mode water layer, as observed in 1964, can be simulated with a regime shift in the forcing. Comparable results have been obtained by Marsh and New (1996). They applied 5 years of anomalous heat flux forcing and found a reduction in the potential vorticity of the mode water during the same period. However, using historical data, we do not find a regime shift in the forcing with a sufficient large amplitude (only the 1970s were anomalously warm, with maxima exceeding 100 W m^{-2}). Outbreaks can increase the amplitude of the response due to the cooling, but the large changes found by TR cannot be attributed to them. Maximum anomalous heat losses in individual years easily exceed 200 W m^{-2}. Due to the ''storage mechanism'' a scenario emerges where a number of very cold years within a longer period can generate a prolonged negative potential vorticity anomaly. The anomaly is formed by the enhanced entrainment due to cooling and subsequent enhanced detrainment due to anomalous low SSTs. In the following years the anomalously stable stratification prevents the anomaly to be attenuated. As shown in experiment VII, in the 1950s no anomaly can be formed because cold and warm winters succeed each other. At the end of the 1950s and in the early 1960s, a number of cold winters induce a persistent negative potential vorticity anomaly, which cannot be attenuated by one warm winter (such as in 1963 or 1967). When in the early 1970s several warm winters succeed each other, the anomaly attenuates. Although most features of TR's time series are reproduced by the model, some differences remain; for example, the onset of the negative potential vorticity anomaly is earlier in the model than in the observations and in 1977 the potential vorticity remains anomalously high. The ''storage mechanism'' could be the reason why TR found the heat loss and mode water formation to be uncorrelated.

It seems that information is carried along the whole subtropical gyre, being able to induce a new anomaly when the old anomaly reaches the western boundary. If the new anomaly is amplified by coupling the ocean model to an atmospheric model or by resolving eddies and reducing the explicit viscous dissipation, this could give a natural timescale for variability in mode water determined by the propagation of anomalies around the gyre.

The anomalous wind stress generates planetary waves that radiate from the eastern boundary. The well-known mechanisms of wave propagation are visible in our model results. The waves propagate to the west. Thickness anomalies near the formation region of mode water are strongly affected by mixed layer processes. The center of the gyre is relatively unaffected.

In the shadow zone the role of advection is small [in the ventilation theory presented by Luyten (1983) the fluid is stagnant], and the imbalance in the forcing induced by the anomalous wind results in planetary wave activity. Consistent with the results of Liu (1993), Rossby waves propagate through the shadow zone (which was not the case in the anomalous heat flux experiments). In the present model the ventilated zone is also affected. According to Liu, in the ventilated zone, the density advection of subducted water tends to cancel a varying Ekman pumping through a barotropic process, resulting in little thermocline variability induced by the wind. However, in the model used here diapycnal processes are included. An imbalance in the forcing can still exist in the ventilated zone, especially in the formation region of mode water where the seasonal cycle in mixed layer depth is large. This is demonstrated by the waves that propagate through the formation zone in the ocean model. Although anomalous wind forcing generates thickness anomalies in the mode water layer, it cannot account for the observed variability in the center of the gyre.

6. Summary and conclusions

The isopycnic model coupled to a mixed layer model simulates a mean circulation that is characteristic for the North Atlantic subtropical gyre. The dominant features of the gyre circulation, the characteristic vertical structure, and the water mass formation processes are fairly well represented. Together with the simple configuration, this makes the model attractive to study variability in thermocline ventilation.

The model equivalent of mode water appears to be a very well ventilated layer. The different regions defined by Luyten et al. (1983) are present in the model solution, but, as evident from the age tracer distribution, ventilation dominates for mode water. There are signs of a pool region where homogenization can take place, but this region is very small. In this region eddy mixing may become important. This issue will be addressed in a later study with an eddy-resolving version of the ocean model.

The main goal of this study was to assess whether variability in the atmospheric forcing can generate mode water variability of the observed amplitude and timescale. In the model used here, both anomalous heat flux forcing and anomalous wind forcing induce thickness anomalies in the mode water layer. However, anomalous heat flux forcing affects the center of the gyre more than anomalous wind forcing does. The anomalous heat flux forcing generates a dipole in the anomalous thickness distribution. Water is lost to a colder layer in the northeast and water is received from a warmer layer in the southwest.

At Panulirus Station, TR observed a drop in potential vorticity of approximately 50×10^{-14} s^{-1} cm^{-1} in the early 1960s. The mode water layer remained in the anomalous state for almost 10 years. As shown in experiments II and III, anomalous heat loss with a maximum of 200 W m^{-2} induces a potential vorticity anom-

aly of 70 $\times$ 10^{-14} s^{-1} cm^{-1} in the mode water layer of the model. The formation of the anomaly in the center of the gyre appears to be mainly determined by local air–sea interactions in conjunction with entrainment and detrainment processes. Advection plays a small role and acts to increase the potential vorticity, in contrast to the hypothesis of TR. Therefore, a prolonged potential vorticity anomaly of the observed timescale can be obtained by a regime shift in the atmosphere forcing (see experiment III). Frequent outbreaks of cold air increase the variability if the average heat loss is anomalously high (see experiment VI). However, no regime shift in the forcing of sufficient amplitude is observed. Therefore, a purely passive ocean cannot explain the observed mode water variability. As the restoration time for an anomalously stable stratification is 5 years after a severe cooling event, an anomaly can persist in the mode water layer, despite interrupting warm years. This defines the storage mechanism. In experiment VII we have shown that potential vorticity anomalies of the observed timescale and amplitude can be generated by anomalous heat losses derived from historical data. The anomalous low potential vorticity in the 1960s and the high potential vorticity in the 1970s are well simulated. It appears that the mechanisms described above operate in the model and generate the prolonged anomalies. The ''storage mechanism'' can be the reason for the lack of correlation between the anomalous heat loss and variability in mode water formation as found by TR. Only in the years when the anomaly is actually formed will the correlation be high.

Not all features of the time series of TR are well simulated, for example, the onset of the negative potential vorticity anomaly in the model occurs too early and the anomalously positive potential vorticity persists in 1977. The model has idealized geometry, idealized forcing, and a coarse resolution, which explain some of the discrepancies with observations. It will be interesting to see how the mechanisms described in the introduction that could not be studied with the present model will modify the results presented here.

Acknowledgments. This research was supported by The Netherlands Organization of Scientific Research (NWO), Project VVA 770-03-252. We thank Dr. G. J. Komen, Dr. A. Kattenberg, and two anonymous reviewers for the comments on the manuscript.

REFERENCES

Bjerknes, J., 1964: Atlantic air/sea interaction. *Advances in Geophysics,* Vol. 10, Academic Press, 1–82.

Bleck, R., and D. B. Boudra, 1986: Wind-driven spin-up in eddy-resolving ocean models formulated in isopynic and isobaric coordinates. *J. Geophys. Res.,* **91,** 7611–7621.

——, H. P. Hanson, D. Hu, and E. B. Kraus, 1989: Mixed layer–thermocline interaction in a three-dimensional isopycnic coordinate model. *J. Phys. Oceanogr.,* **19,** 1417–1439.

Cayan, D. R., 1992: Latent and sensible heat flux anomalies over the northern oceans: Driving the sea surface temperature. *J. Phys. Oceanogr.,* **22,** 1417–1439.

Cox, M. D., 1987: An eddy resolving numerical model of the ventilated thermocline: Time dependence. *J. Phys. Oceanogr.,* **17,** 1044–1056.

Dickson, R., J. Lazier, J. Meincke, P. Rhines, and J. Swift, 1996: Long-term coordinated changes in the convective activity of the North Atlantic. *Progress in Oceanography,* Vol. 38, Pergamon, 241–295.

Drijfhout, S. S., 1994a: Heat transport by mesoscale eddies in an ocean circulation model. *J. Phys. Oceanogr.,* **24,** 353–369.

——, 1994b: Sensitivity of eddy-induced heat transport to diabatic forcing. *J. Geophys. Res.,* **99,** 18 481–18 499.

——, and F. H. Walsteijn, 1998: Eddy-induced heat transport in a coupled ocean–atmospheric anomaly model. *J. Phys. Oceanogr.,* **28,** 250–265.

Griffies, S. M., and E. Tziperman, 1995: A linear oscillator driven by stochastic atmospheric forcing. *J. Climate,* **8,** 2440–2453.

Hasselmann, K., 1976: Stochastic climate models. Part I. Theory. *Tellus,* **28,** 473–485.

Huang, R. X., 1990: Does atmospheric cooling drive the Gulf Stream recirculation? *J. Phys. Oceanogr.,* **20,** 751–757.

——, and K. Bryan, 1987: A multilayer model of the thermohaline and wind-driven ocean circulation. *J. Phys. Oceanogr.,* **17,** 1909–1924.

Jenkins, W. J., 1982: On the climate of a subtropical ocean gyre: Decade timescale variations in water mass renewal in the Sargasso Sea. *J. Mar. Res.,* **40** (Suppl.), 265–290.

——, 1988: The use of anthropogenic tritium and helium-3 to study subtropical gyre ventilation and circulation. *Philos. Trans. Roy. Soc. London Ser. A,* **325,** 43–61.

Jiang, S, F. F. Jin, and M. Ghil, 1995: Multiple equilibria, periodic, and aperiodic solutions in a wind-driven, double gyre, shallow-water model. *J. Phys. Oceanogr.,* **25,** 764–786.

Joyce, T. M. and P. Robbins, 1996: The long-term hydrographic record at Bermuda. *J. Climate,* **9,** 3121–3131

Kushnir, Y., 1994: Interdecadal variations in North Atlantic sea surface temperature and associated atmospheric conditions. *J. Climate,* **7,** 141–157.

Latif, M., and T. P. Barnett, 1996: Decadal climate variability over the North Pacific and North America: Dynamics and predictability. *J. Climate,* **9,** 2407–2423

Liu, Z., 1993: Thermocline forced by varying Ekman pumping. Part II: Annual and decadal Ekman pumping. *J. Phys. Oceanogr.,* **23,** 2523–2540.

Luyten, J. R., J. Pedlosky, and H. Stommel, 1983: The ventilated thermocline. *J. Phys. Oceanogr.,* **13,** 292–309.

Marsh, R., and A. L. New, 1996: Modeling 18° Water variability. *J. Phys. Oceanogr.,* **26,** 1059–1080.

Marshall, J. C., A. J. G Nurser, and R. G. Williams, 1993: Inferring the subduction rate and period over the North Atlantic. *J. Phys. Oceanogr.,* **23,** 1315–1329.

Martin, P. J., 1985: Simulation of the mixed layer at OWS November and Papa with several models. *J. Geophys. Res,* **90,** 903–916.

McCartney, M. S., 1982: The subtropical recirculation of Mode Waters. *J. Mar. Res.,* **40** (Suppl.), 427–464.

Pedlosky, J., 1987: *Geophysical Fluid Dynamics.* Springer-Verlag, 710 pp.

Qiu, B., and R. X. Huang, 1995: Ventilation of the North Atlantic and North Pacific: Subduction versus obduction. *J. Phys. Oceanogr.,* **25,** 2374–2390.

Rhines, P. B., and W. R. Young, 1982: Homogenization of potential vorticity in planetary gyres. *J. Fluid Mech.,* **122,** 347–367.

Semtner, A. J., and Y. Mintz, 1977: Numerical simulation of the Gulf Stream and mid-ocean eddies. *J. Phys. Oceanogr.,* **7,** 208–230.

Speer, K., and E. Tziperman, 1992: Rates of water mass formation in the North Atlantic Ocean. *J. Phys. Oceanogr.,* **22,** 93–104.

Speich, S., H. Dijkstra, and M. Ghil, 1995: Successive bifurcations in a shallow-water model applied to the wind-driven ocean circulation. *Nonlin. Proc. Geophys.,* **2,** 241–268.

Sterl, A., and A. Kattenberg, 1994: Embedding a mixed model in an

ocean general circulation model of the Atlantic: The importance of surface mixing for heat flux and temperature. *J. Geophys. Res.*, **99,** 14 139–14 157.

Talley, L. D., and M. E. Raymer, 1982: Eighteen degree water variability. *J. Mar. Res.*, **40** (Suppl.), 757–775.

Williams, R. G., M. A. Spall, and J. C. Marshall, 1995: Does Stommel's mixed layer ''Demon'' work? *J. Phys. Oceanogr.*, **25,** 3089–3102.

Woodruff, S. D., R. J. Slutz, R. L. Jenne, and P. M. Steurer, 1987: A Comprehensive Ocean–Atmosphere Data Set. *Bull. Amer. Meteor. Soc.*, **68,** 521–527.

Woods, J. D., 1985: The physics of thermocline ventilation. *Coupled Ocean–Atmosphere Models*, J. C. J. Nihoul, Ed., Elsevier, 543–590.

Worthington, L. V., 1959: The 18° water in the Sargasso Sea. *Deep-Sea Res.*, **5,** 297–305.